Communications on Applied Mathematics and Computation
https://doi.org/10.1007/s42967-023-00313-6

ORIGINAL PAPER

# High-Order ADER Discontinuous Galerkin Schemes for a Symmetric Hyperbolic Model of Compressible Barotropic Two-Fluid Flows

**Laura Río-Martín**[1,2] · **Michael Dumbser**[1]

Received: 28 March 2023 / Revised: 31 July 2023 / Accepted: 24 August 2023
© The Author(s) 2023

**Abstract**
This paper presents a high-order discontinuous Galerkin (DG) finite-element method to solve the barotropic version of the conservative symmetric hyperbolic and thermodynamically compatible (SHTC) model of compressible two-phase flow, introduced by Romenski et al. in [59, 62], in multiple space dimensions. In the absence of algebraic source terms, the model is endowed with a curl constraint on the relative velocity field. In this paper, the hyperbolicity of the system is studied for the first time in the multidimensional case, showing that the original model is only weakly hyperbolic in multiple space dimensions. To restore the strong hyperbolicity, two different methodologies are used: (i) the explicit symmetrization of the system, which can be achieved by adding terms that contain linear combinations of the curl involution, similar to the Godunov-Powell terms in the MHD equations; (ii) the use of the hyperbolic generalized Lagrangian multiplier (GLM) curl-cleaning approach forwarded. The PDE system is solved using a high-order ADER-DG method with *a posteriori* subcell finite-volume limiter to deal with shock waves and the steep gradients in the volume fraction commonly appearing in the solutions of this type of model. To illustrate the performance of the method, several different test cases and benchmark problems have been run, showing the high order of the scheme and the good agreement when compared to reference solutions computed with other well-known methods.

**Keywords** Compressible two-fluid flows · Symmetric hyperbolic and thermodynamically compatible (SHTC) systems · Hyperbolic systems with curl involutions · High-order ADER discontinuous Galerkin (DG) schemes with subcell finite-volume limiter · Conservative form of hyperbolic models

**Mathematics Subject Classification** 65M60 · 35L65 · 76T10

This paper is dedicated to Gerald Warnecke at the occasion of his 65th birthday and in honor of his groundbreaking scientific contributions to the field of numerical methods for hyperbolic PDE. The authors are also very grateful for the friendship and all the inspiring discussions over the years.

Extended author information available on the last page of the article

## 1 Introduction

Multi-phase flows are ubiquitous in nature and engineering applications. The simplest flow of a liquid with free surface, such as a flowing river or a falling raindrop, already involves both the dynamics of the liquid phase and the surrounding air and can consequently be considered a two-phase flow. The application range is obviously much larger and includes, for example, and without pretending to be exhaustive, bubbly liquids and sprays, water flow with sediment transport, mist flows, two-phase flows with phase change as used in modern 3D printers, compressible multi-phase flows in internal combustion engines, flows in the paper, steel and food industry, etc. Such applications have motivated extensive efforts to study and develop multi-phase flow models that describe such phenomena with respect to physical principles and thermodynamics.

One particular aspect of multi-phase flows is that they involve moving interfaces between different bulk phases. From a physics perspective, the nature of the interface, that is, whether it is sharp or diffuse, has been subject to debate since the times of Rayleigh and Laplace. While both approaches have their advantages, it is admitted that diffuse interface approaches, in general, offer more flexibility, especially in the presence of strong deformations and topology changes in the interface geometry. In contrast, the sharp interface approach allows for a more rigorous treatment of the thermodynamics at the interface. In this paper, we are interested in diffuse interface approaches. Although a thorough review of diffuse interface approaches is beyond the scope of this work, the reader is, for example, referred to [1, 2, 7, 10, 18, 35, 36, 39, 46, 47, 50, 55, 65, 75] and references therein. For the incompressible case, see also [14, 37, 38] and related work.

Up to now, no universally accepted mathematical model exists for the whole range of different compressible multi-phase flows. Among the large number of different models that can be found in the literature, the one proposed by Baer and Nunziato [4] is one of the most widespread, see, for example, [3, 8, 41, 65], as well as the well-known Kapila model [46], which can be obtained from the Baer-Nunziato (BN) model in the stiff relaxation limit. The governing equations of the BN model form a hyperbolic system, because the associated eigenvalues are all real, and there exists a set of linearly independent eigenvectors. However, some of its equations cannot be written in the conservative form, which makes it difficult to deal with the appearance of discontinuities and the development of high-order numerical methods. Moreover, the BN model was modified by different authors in the literature, see, for example, Saurel and Abgrall [65], whose modification describes multi-phase mixtures and interface problems between pure compressible materials. An alternative two-phase flow model that is fully conservative is the one forwarded by Scannapieco and Cheng, see [66].

In addition to the previously mentioned models, there exists another class of models for compressible multi-phase flows that originates from the theory of Godunov and Romenski on symmetric hyperbolic and thermodynamically compatible (SHTC) systems [42, 44, 56, 57] and which was first introduced in [58, 59, 62, 63]. In this paper, we are therefore interested in the discretization of the SHTC model of *barotropic* compressible two-phase flows of Romenski et al. with different phase velocities and phase pressures in multiple space dimensions. The model consists of a first-order SHTC system of equations [58, 59, 62]. In the previous references, it was also shown that the SHTC equations, which are written in the conservative form, can be converted to the form of a BN-type model, where additional differential terms appear in the momentum equations, which were not included in the original BN model and which describe the so-called lift forces. Recently, an exact solution for

the corresponding Riemann problem in the barotropic case was found in [69], and an all-Mach number flow solver was developed in [48].

The model proposed by Romenski et al. is strongly hyperbolic in one space dimension, and its homogeneous part without algebraic source terms is endowed with a curl involution on the relative velocity field. However, as we will show in this paper, the original model is only weakly hyperbolic in multiple space dimensions. To restore strong hyperbolicity, two different strategies can be followed: the first one consists in using the hyperbolic generalized Lagrangian multiplier (GLM) curl-cleaning methodology introduced in [11, 16, 20, 29], which is a natural extension of the original ideas presented by Munz et al. in [19, 49] on hyperbolic GLM divergence cleaning for the Maxwell and MHD equations, which contain the well-known divergence-free condition of the magnetic field. Curl constraints can also be found in many other first-order hyperbolic models, such as hyperbolic models for surface tension [15, 16, 67], first-order hyperbolic reformulations of the Navier-Stokes-Korteweg equations based on an augmented Lagrangian approach [20, 21], or first-order reductions of the Einstein field equations of general relativity [29]. The second methodology to recover the hyperbolicity involves the use of some extra terms in the momentum equation that symmetrize the system and is therefore directly based on the theory of SHTC systems following [43, 52–54]. In both cases, we will show that the system in the multidimensional case becomes again strongly hyperbolic.

In the setting of this model, the solutions are often discontinuous in space, that is, solutions to Riemann problems. Therefore, it is necessary to consider an approach that is robust and accurate even in the presence of shock waves or discontinuities. To address the sharp gradients of the numerical solutions, a high-order ADER discontinuous Galerkin (DG) finite-element framework with *a posteriori* subcell finite-volume limiter is considered, see [27, 34, 76] for further details. The proposed method is high order in space and time, thanks to the use of the ADER approach of Toro and Titarev [70, 73, 74]. To deal with spurious oscillations that may appear in the presence of discontinuities or shock waves, it makes use of *a posteriori* subcell finite-volume limiter for high-order fully discrete one-step ADER-DG schemes presented in [34, 76], which follows the multi-dimensional optimal order detection (MOOD) approach of Clain and Loubère [17, 22, 23].

This paper is organized as follows. Section 2 recalls the set of governing partial differential equations and shows the equation of state (EOS) that we will use in this work. In Sect. 2.2, the hyperbolicity of the system is studied in the multidimensional case, showing that the original model is only weakly hyperbolic, and two different strategies to recover strong hyperbolicity are presented. Section 3 introduces the high-order ADER-DG scheme used in this paper to solve the model numerically. Section 4 shows the results of several test cases and benchmark problems computed using the proposed method. Finally, Sect. 5 concludes the paper and summarizes the contributions of this work as well as its possible future extensions.

## 2 Governing Equations

The governing equations of the barotropic compressible two-velocity, two-pressure two-fluid model of Romenski, written in terms of the specific total energy potential $E = E(\alpha_1, c_1, \rho, w^k)$ are given by

$$
\begin{cases}
\dfrac{\partial \rho\alpha_1}{\partial t} + \dfrac{\partial \rho\alpha_1 u^k}{\partial x_k} = -\dfrac{\rho}{\tau} E_{\alpha_1}, & \text{(1a)}\\
\dfrac{\partial \rho c_1}{\partial t} + \dfrac{\partial (\rho c_1 u^k + \rho E_{w^k})}{\partial x_k} = 0, & \text{(1b)}\\
\dfrac{\partial \rho}{\partial t} + \dfrac{\partial \rho u^k}{\partial x_k} = 0, & \text{(1c)}\\
\dfrac{\partial \rho u^i}{\partial t} + \dfrac{\partial (\rho u^i u^k + p\delta_{ik} + \rho w^i E_{w^k})}{\partial x_k} = g^i \rho, & \text{(1d)}\\
\dfrac{\partial w^k}{\partial t} + \dfrac{\partial (w^l u^l + E_{c_1})}{\partial x_k} + u^l \left( \dfrac{\partial w^k}{\partial x_l} - \dfrac{\partial w^l}{\partial x_k} \right) = -\zeta E_{w_k}, & \text{(1e)}
\end{cases}
$$

where $\alpha_1$ and $\alpha_2$ are the volume fractions of the first and second phases, verifying the saturation constraint $\alpha_1 + \alpha_2 = 1$, $\rho_1$ and $\rho_2$ are the mass densities of the first and second phases, $\rho = \alpha_1\rho_1 + \alpha_2\rho_2$ is the mixture mass density, $c_j = \alpha_j\rho_j/\rho$ with $j = 1, 2$ are the mass fractions of phase $j$ which satisfy $c_1 + c_2 = 1$, and $\boldsymbol{g} = (g^1, g^2, g^3)^{\mathrm{T}}$ is the gravity acceleration. If $\boldsymbol{u}_1 = (u_1^1, u_1^2, u_1^3)^{\mathrm{T}}$ and $\boldsymbol{u}_2 = (u_2^1, u_2^2, u_2^3)^{\mathrm{T}}$ are the velocity vectors of each phase, then the mixture velocity $\boldsymbol{u} = (u^1, u^2, u^3)^{\mathrm{T}}$ is computed as $u^k = c_1 u_1^k + c_2 u_2^k$ and the relative phase velocity, which is a primary evolution quantity in this model, is given by $\boldsymbol{w} = (w^1, w^2, w^3)^{\mathrm{T}}$ as $w^k = u_1^k - u_2^k$. The source terms of Eqs. (1a) and (1e) are proportional to thermodynamic forces with $\tau$ the rate of pressure relaxation and $\zeta$ the inter-phase friction coefficient. The PDE system (1) is formed by two conservation laws for the volume and mass fractions, Eqs. (1a) and (1b), respectively, the conservation of the total mass, Eq. (1c), the conservation of the mixture momentum, Eq. (1d), and a balance law for the relative velocity, Eq. (1e). The algebraic source terms appearing in Eqs. (1a) and (1e) describe the interaction between the phases and are pressure relaxation and interfacial friction. The mixture EOS is given by, see [69],

$$
E(\alpha_1, c_1, \rho, w^1, w^2, w^3) = e(\alpha_1, c_1, \rho) + c_1 c_2 \frac{w^i w^i}{2},
$$

where the specific internal energy of the mixture reads as

$$
e(\alpha_1, c_1, \rho) = c_1 e_1(\rho_1) + c_2 e_2(\rho_2) = c_1 e_1\left(\frac{c_1\rho}{\alpha_1}\right) + c_2 e_2\left(\frac{c_2\rho}{\alpha_2}\right),
$$

where $e_j(\rho_j)$ is the specific internal energy of the phase $j$. Since, in this work, an isentropic process is considered, the derivatives of $e$ can be computed as

$$
\frac{\partial e}{\partial \alpha_1} = \frac{p_2 - p_1}{\rho}, \qquad \frac{\partial e}{\partial c_1} = h_1(\rho_1) - h_2(\rho_2), \qquad \frac{\partial e}{\partial \rho} = \frac{p}{\rho^2},
$$

where $h_j(\rho_j) = e_j(\rho_j) + \frac{p_j(\rho_j)}{\rho_j}$, $j = 1, 2$ is the specific enthalpy of the phase $j$. Then, the derivatives of the specific total energy $E$ are given by

$$\frac{\partial E}{\partial \alpha_1} = \frac{\partial e}{\partial \alpha_1} = \frac{p_2 - p_1}{\rho}, \quad \frac{\partial E}{\partial \rho} = \frac{\partial e}{\partial \rho} = \frac{p}{\rho^2}, \quad \frac{\partial E}{\partial w^i} = c_1(1-c_1)w^i, \tag{2}$$

$$\frac{\partial E}{\partial c_1} = \frac{\partial e}{\partial c_1} + (1-2c_1)\frac{w^i w^i}{2} = h_1(\rho_1) - h_2(\rho_2) + (1-2c_1)\frac{w^i w^i}{2}. \tag{3}$$

Considering the computations in [69], and taking into account (2) and (3), the following identities are obtained:

$$\begin{aligned}
&\rho c_1 u^k + \rho E_{w^k} = \rho c_1 u_1^k, \quad \rho c_2 u^k - \rho E_{w^k} = \rho c_2 u_2^k,\\
&\rho u^i u^k + p\delta_{ik} + \rho w^i E_{w^k} = \alpha_1 \rho_1 u_1^i u_1^k + \alpha_2 \rho_2 u_2^i u_2^k + p\delta_{ik},\\
&(u_1^l - u_2^l)u^l + E_{c_1} = \frac{1}{2}(u_1^l)^2 - \frac{1}{2}(u_2^l)^2 + h_1 - h_2.
\end{aligned}$$

The PDE system (1) can now be rewritten in the following form, which is more convenient for numerical discretization:

$$\begin{cases}
\dfrac{\partial \alpha_1}{\partial t} + u^k \dfrac{\partial \alpha_1}{\partial x_k} = -\dfrac{p_2 - p_1}{\tau \rho}, & \text{(4a)}\\
\dfrac{\partial \alpha_1 \rho_1}{\partial t} + \dfrac{\partial (\alpha_1 \rho_1 u_1^k)}{\partial x_k} = 0, & \text{(4b)}\\
\dfrac{\partial \alpha_2 \rho_2}{\partial t} + \dfrac{\partial (\alpha_2 \rho_2 u_2^k)}{\partial x_k} = 0, & \text{(4c)}\\
\dfrac{\partial \rho u^i}{\partial t} + \dfrac{\partial (\alpha_1 \rho_1 u_1^i u_1^k + \alpha_2 \rho_2 u_2^i u_2^k + p\delta_{ik})}{\partial x_k} = g^i \rho, & \text{(4d)}\\
\dfrac{\partial w^k}{\partial t} + \dfrac{\partial}{\partial x_k}\left(\dfrac{1}{2}(u_1^l)^2 - \dfrac{1}{2}(u_2^l)^2 + h_1 - h_2\right) + u^l\left(\dfrac{\partial w^k}{\partial x_l} - \dfrac{\partial w^l}{\partial x_k}\right) = -\zeta c_1 c_2 w^k. & \text{(4e)}
\end{cases}$$

The derivation of the PDE system (4) is based on the principles of thermodynamically compatible systems [44], and it consists of nine equations: the balance law for the volume fraction, the conservation laws of the two-phase masses, the conservation of the mixture momentum, and the balance law for the relative velocity field. Note that in the absence of source terms in (4e), i.e., for $\zeta = 0$, the relative velocity is curl-free in the sense

$$\frac{\partial w^k}{\partial x_l} - \frac{\partial w^l}{\partial x_k} = 0.$$

## 2.1 EOS

To close the two-phase model (4a)–(4e), it is necessary to define an EOS for each phase: throughout this paper, we will make use either of the ideal gas law or of the stiffened gas EOS, which will be used to model a liquid phase. For ideal gases, the EOS is defined as

$$E(\rho) = \frac{c_0^2}{\gamma(\gamma-1)} \quad \text{with } c_0^2 = \gamma\rho^{\gamma-1}\mathrm{e}^{s/c_v}, \tag{5}$$

where $\gamma$ is the adiabatic index or the ratio of specific heats, $c_0$ is the adiabatic sound speed, $s$ is the specific entropy (which in our case will be constant), $c_v$ is the specific heat capacity at constant volume, and the pressure is given by

$$p(\rho) = \rho^2 E_\rho = \rho^\gamma \mathrm{e}^{s/c_v} = (\gamma-1)\rho E. \tag{6}$$

For stiffened gases, the EOS reads as

$$E(\rho) = \frac{c_0^2}{\gamma(\gamma-1)}\left(\frac{\rho}{\rho_0}\right)^{\gamma-1}\mathrm{e}^{s/c_v} + \frac{\rho_0 c_0^2 - \gamma p_0}{\gamma\rho}, \tag{7}$$

where $\rho_0$ and $p_0$ are the reference density and pressure, respectively, and $c_0$ is a constant reference sound speed. In this case, the pressure is computed as

$$p(\rho) = \rho^2 E_\rho = \frac{c_0^2\rho_0}{\gamma}\left(\frac{\rho}{\rho_0}\right)^{\gamma}\mathrm{e}^{s/c_v} - \frac{c_0^2\rho_0 - \gamma p_0}{\gamma}. \tag{8}$$

### 2.2 Hyperbolicity Analysis

In this section, we will study the hyperbolicity of the model (4a)–(4e). The one-dimensional (1D) case was already addressed in [69], and here, we briefly recall some results for the 1D case before moving to the more general multidimensional case. In particular, we will prove that the original system (4a)–(4e) is only *weakly hyperbolic* in the multidimensional case and show how the strong hyperbolicity can be restored considering two different strategies: on the one hand, using an extension of the hyperbolic GLM curl-cleaning approach, and on the other hand, modifying the original system of governing equations by adding the symmetrizing terms that allow rewriting the model in symmetric hyperbolic form, which is natural within the framework of SHTC equations. Defining the vectors of conserved and primitive variables as $\mathbf{Q} = (\alpha_1, \alpha_1\rho_1, \alpha_2\rho_2, \rho\boldsymbol{u}^{\mathrm{T}}, \boldsymbol{w}^{\mathrm{T}})^{\mathrm{T}}$ and $\mathbf{V} = (\alpha_1, \rho_1, \rho_2, \boldsymbol{u}_1^{\mathrm{T}}, \boldsymbol{u}_2^{\mathrm{T}})^{\mathrm{T}}$, respectively, the PDE system (4) can be written as

$$\partial_t\mathbf{Q} + \nabla\cdot\mathbf{F}(\mathbf{Q}) + \mathbf{B}(\mathbf{Q})\cdot\nabla\mathbf{Q} = \mathbf{S}(\mathbf{Q}),$$

where $\mathbf{S}(\mathbf{Q})$ contains the source terms, $\mathbf{F}(\mathbf{Q})$ is the nonlinear flux tensor, and $\mathbf{B}(\mathbf{Q})\cdot\nabla\mathbf{Q}$ contains the non-conservative terms. Then, the quasi-linear form of the PDE in terms of the conserved variables $\mathbf{Q}$ is given by

$$\partial_t\mathbf{Q} + \mathbf{A}(\mathbf{Q})\cdot\nabla\mathbf{Q} = \mathbf{S}(\mathbf{Q}),$$

where $\mathbf{A}(\mathbf{Q}) = \dfrac{\partial\mathbf{F}}{\partial\mathbf{Q}} + \mathbf{B}$. If the vector of primitive variables $\mathbf{V}$ is considered, the system can be written as

$$\partial_t \mathbf{V} + \mathbf{C}(\mathbf{V}) \cdot \nabla \mathbf{V} = \boldsymbol{\mathcal{S}}(\mathbf{V}), \tag{9}$$

where $\mathbf{C}(\mathbf{V}) = \dfrac{\partial \mathbf{V}}{\partial \mathbf{Q}} \dfrac{\partial \mathbf{F}}{\partial \mathbf{V}} + \dfrac{\partial \mathbf{V}}{\partial \mathbf{Q}} \mathbf{B} \dfrac{\partial \mathbf{Q}}{\partial \mathbf{V}}$ and $\boldsymbol{\mathcal{S}}(\mathbf{V}) = \dfrac{\partial \mathbf{V}}{\partial \mathbf{Q}} \mathbf{S}(\mathbf{Q})$. Throughout this section, for the sake of the readability and since it does not contribute anything to the study of the hyperbolicity of the system, the source terms are set to 0.

### 2.2.1 1D Case

The hyperbolicity analysis of the system (4) in one dimension has been done in detail in [69], so here, only a summary of the main points will be made that will be useful for a better understanding of the multidimensional case. If $u = c_1 u_1 + c_2 u_2$ is the mixture velocity with $u_j$, $j = 1, 2$ the velocity of the phase $j$ and $w = u_1 - u_2$ is the relative velocity, the 1D system results in

Then, the matrix $\mathbf{C}$ in (9) is given by

$$\begin{cases} \dfrac{\partial \alpha_1}{\partial t} + u \dfrac{\partial \alpha_1}{\partial x} = 0, & \text{(10a)} \\ \dfrac{\partial \alpha_1 \rho_1}{\partial t} + \dfrac{\partial (\alpha_1 \rho_1 u_1)}{\partial x} = 0, & \text{(10b)} \\ \dfrac{\partial \alpha_2 \rho_2}{\partial t} + \dfrac{\partial (\alpha_2 \rho_2 u_2)}{\partial x} = 0, & \text{(10c)} \\ \dfrac{\partial \rho u}{\partial t} + \dfrac{\partial (\alpha_1 \rho_1 (u_1)^2 + \alpha_2 \rho_2 (u_2)^2 + p)}{\partial x} = 0, & \text{(10d)} \\ \dfrac{\partial w}{\partial t} + \dfrac{\partial}{\partial x} \left( \dfrac{1}{2}(u_1)^2 - \dfrac{1}{2}(u_2)^2 + h_1 - h_2 \right) = 0. & \text{(10e)} \end{cases}$$

$$\mathbf{C}(\mathbf{V}) = \begin{pmatrix} u & 0 & 0 & 0 & 0 \\ \frac{\rho_1}{\alpha_1}(u_1 - u) & u_1 & 0 & \rho_1 & 0 \\ \frac{\rho_2}{\alpha_2}(u - u_2) & 0 & u_2 & 0 & \rho_2 \\ \beta & \frac{a_1^2}{\rho_1} & 0 & u_1 & 0 \\ \beta & 0 & \frac{a_2^2}{\rho_2} & 0 & u_2 \end{pmatrix}$$

with $a_j$ the sound speed of phase $j$, that is defined as $a_j^2 = \rho_j \left( \frac{\partial h_j}{\partial \rho_j} \right)$, $j = 1, 2$ and $\beta = \frac{1}{\rho} \left( \frac{a_1^2 \rho_1}{\gamma_1} - \frac{a_2^2 \rho_2}{\gamma_2} \right) = \frac{1}{\rho}(p_1 - p_2)$. It is easy to show that $\mathbf{C}(\mathbf{V})$ admits five eigenvalues, whose expressions are given hereafter

$$\lambda_1 = u_1 + a_1,\ \lambda_2 = u_1 - a_1,\ \lambda_3 = u,\ \lambda_4 = u_2 + a_2,\ \lambda_5 = u_2 - a_2.$$

In this case, all five eigenvalues are real, and a complete set of five linearly independent eigenvectors exists, which means that the system in one space dimension is *strongly hyperbolic*, see [69] for further details about the eigenvalues and eigenvectors in the 1D case.

### 2.2.2 Multidimensional Case

Now, we are in the position to study the multidimensional case. In the following, we use the property of *rotational invariance* of Newtonian mechanics, and hence, it is enough to consider the matrix $\mathbf{C}(\mathbf{V})$ only in the $x$-direction and not all possible space directions. The system under consideration is (4) and, in this case, the matrix $\mathbf{C}(\mathbf{V})$ in the $x$-direction is given by

$$\mathbf{C}(\mathbf{V}) = \begin{pmatrix} u^1 & 0 & 0 & 0 & 0 & 0 & 0 & 0 & 0 \\ \frac{\rho_1}{\alpha_1}\vartheta_2^1 & u_1^1 & 0 & \rho_1 & 0 & 0 & 0 & 0 & 0 \\ \frac{\rho_2}{\alpha_2}\vartheta_1^1 & 0 & u_2^1 & 0 & 0 & 0 & \rho_2 & 0 & 0 \\ \beta & \frac{a_1^2}{\rho_1} & 0 & u_1^1 & \vartheta_{22}^2 & \vartheta_{22}^3 & 0 & \vartheta_{12}^2 & \vartheta_{12}^3 \\ 0 & 0 & 0 & 0 & \xi_2 & 0 & 0 & -\vartheta_{12}^1 & 0 \\ 0 & 0 & 0 & 0 & 0 & \xi_2 & 0 & 0 & -\vartheta_{12}^1 \\ \beta & 0 & \frac{a_2^2}{\rho_2} & 0 & -\vartheta_{12}^2 & -\vartheta_{12}^3 & u_2^1 & -\vartheta_{11}^2 & -\vartheta_{11}^3 \\ 0 & 0 & 0 & 0 & \vartheta_{12}^1 & 0 & 0 & \xi_1 & 0 \\ 0 & 0 & 0 & 0 & 0 & \vartheta_{12}^1 & 0 & 0 & \xi_1 \end{pmatrix}.$$

As in the previous section, we make use of the following auxiliary variables to ease the expressions in the matrix:

$$\begin{cases} \beta = \frac{1}{\rho}(p_1 - p_2), \\ \vartheta_j^i = c_j w^i,\ \vartheta_{jk}^i = c_j c_k w^i,\ i = 1,2,3,\ j = 1,2,\ k = 1,2, \\ \xi_1 = c_1 u^1 + c_2 u_2^1 = u_2^1 + c_1^2 w^1 = u_2^1 + c_1 \vartheta_1^1, \\ \xi_2 = c_1 u_1^1 + c_2 u^1 = u_1^1 - c_2^2 w^1 = u_1^1 - c_2 \vartheta_2^1. \end{cases} \tag{11}$$

The matrix $\mathbf{C}$ admits 9 eigenvalues $\lambda_{1-9}$ that are given by

$$\lambda_1 = u_1^1 - a_1,\ \lambda_2 = u_1^1 + a_1,\ \lambda_3 = u_2^1 - a_2,\ \lambda_4 = u_2^1 + a_2,\ \lambda_{5-9} = u^1,$$

where the sound speed of each phase $a_j$ again is defined as $a_j^2 = \rho_i\left(\frac{\partial h_j}{\partial \rho_j}\right)$, $j = 1,2$. The eigenvalues are all real. To prove whether the system is weakly or strongly hyperbolic, it is necessary to compute the associated eigenvectors. The right eigenvectors are the columns in the matrix below and are given in the same order as the eigenvalues

$$\mathbf{R}_{1-4} = \begin{pmatrix} 0 & 0 & 0 & 0 \\ -\frac{\rho_1}{a_1} & \frac{\rho_1}{a_1} & 0 & 0 \\ 0 & 0 & -\frac{\rho_2}{a_2} & \frac{\rho_2}{a_2} \\ 1 & 1 & 0 & 0 \\ 0 & 0 & 0 & 0 \\ 0 & 0 & 0 & 0 \\ 0 & 0 & 1 & 1 \\ 0 & 0 & 0 & 0 \\ 0 & 0 & 0 & 0 \end{pmatrix}, \quad \mathbf{R}_{5-7} = \begin{pmatrix} -\frac{\alpha_1 \alpha_2 Z_2}{\eta_2 \vartheta_1^1} & 0 & 0 \\ \frac{\rho_1 \zeta_1 Z_2}{\eta_2 \vartheta_1^1 Z_1} & -\frac{\rho_1 \vartheta_2^3}{Z_1} & -\frac{\rho_1 \vartheta_2^2}{Z_1} \\ \frac{\rho_2 \zeta_2}{\eta_2 \vartheta_1^1} & \frac{\rho_2 \vartheta_1^3}{Z_2} & \frac{\rho_2 \vartheta_1^2}{Z_2} \\ -\frac{c_2 \eta_1 \vartheta_2^1}{c_1 \eta_2 Z_1} & \frac{\vartheta_2^1 \vartheta_2^3}{Z_1} & \frac{\vartheta_2^1 \vartheta_2^2}{Z_1} \\ 0 & 0 & 1 \\ 0 & 1 & 0 \\ 1 & \frac{\vartheta_1^1 \vartheta_1^3}{Z_2} & \frac{\vartheta_1^1 \vartheta_1^2}{Z_2} \\ 0 & 0 & 1 \\ 0 & 1 & 0 \end{pmatrix},$$

where the auxiliary variables that are used to ease the notation are defined as

$$Z_1 = a_1^2 - (\vartheta_2^1)^2, \quad Z_2 = a_2^2 - (\vartheta_1^1)^2, \quad \eta_1 = \alpha_2(a_1^2 - \alpha_1\beta),$$
$$\eta_2 = \alpha_1(a_2^2 + \alpha_2\beta), \quad \zeta_1 = \alpha_2\left(\alpha_1\beta - (\vartheta_2^1)^2\right), \quad \zeta_2 = \alpha_1\left(\alpha_2\beta + (\vartheta_1^1)^2\right).$$

All eigenvalues are real, but two eigenvectors are missing (in fact, if we are working in dimension $d$, there are $d-1$ missing eigenvectors), so the system is only *weakly hyperbolic*. Hereafter, we will show two different methodologies that can be used to restore the strong hyperbolicity of the model.

**2.2.2.1 GLM Curl-Cleaning Approach** To restore the strong hyperbolicity and following the same strategy that can be found in [11, 16, 20, 29], we make use of the GLM curl-cleaning technique, where an evolution equation for a curl-cleaning field $\psi^k$ is added to the system (4). Using the abbreviation $\delta_{12} = \frac{1}{2}(u_1^l)^2 - \frac{1}{2}(u_2^l)^2 + h_1 - h_2$ and denoting the curl-cleaning speed by $a_{\psi}$, this equation is coupled with (4e) via a Maxwell-type sub-system as follows:

$$\begin{cases} \dfrac{\partial w^k}{\partial t} + \dfrac{\partial \delta_{12}}{\partial x_k} + u^l\left(\dfrac{\partial w^k}{\partial x_l} - \dfrac{\partial w^l}{\partial x_k}\right) + a_{\psi}\varepsilon_{klm}\dfrac{\partial \psi^m}{\partial x_l} = 0, \\ \dfrac{\partial \psi^k}{\partial t} + u^j\dfrac{\partial \psi^k}{\partial x_j} - a_{\psi}\varepsilon_{klm}\dfrac{\partial w^m}{\partial x_l} = 0. \end{cases}$$

Hence, the augmented system with GLM curl-cleaning reads

$$\frac{\partial \alpha_1}{\partial t} + u^k\frac{\partial \alpha_1}{\partial x_k} = 0, \tag{12a}$$

$$\frac{\partial \alpha_1\rho_1}{\partial t} + \frac{\partial(\alpha_1\rho_1 u_1^k)}{\partial x_k} = 0, \tag{12b}$$

$$\frac{\partial \alpha_2\rho_2}{\partial t} + \frac{\partial(\alpha_2\rho_2 u_2^k)}{\partial x_k} = 0, \tag{12c}$$

$$\frac{\partial \rho u^i}{\partial t} + \frac{\partial (\alpha_1 \rho_1 u_1^i u_1^k + \alpha_2 \rho_2 u_2^i u_2^k + p\delta_{ik})}{\partial x_k} = 0, \tag{12d}$$

$$\frac{\partial w^k}{\partial t} + \frac{\partial \delta_{12}}{\partial x_k} + u^l \left( \frac{\partial w^k}{\partial x_l} - \frac{\partial w^l}{\partial x_k} \right) + a_\psi \varepsilon_{klm} \frac{\partial \psi^m}{\partial x_l} = 0, \tag{12e}$$

$$\frac{\partial \psi^k}{\partial t} + u^j \frac{\partial \psi^k}{\partial x_j} - a_\psi \varepsilon_{klm} \frac{\partial w^m}{\partial x_l} = 0, \tag{12f}$$

where $\boldsymbol{\psi} = (\psi^1, \psi^2, \psi^3)$ is the cleaning field, $\boldsymbol{\varepsilon} = \varepsilon_{klm}$ is the Levi-Civita tensor, and $a_\psi$ is the curl-cleaning speed. Once the curl-cleaning field has been added, we can compute the eigenvalues and eigenvectors to check the hyperbolicity of the augmented GLM system. The matrix $\mathbf{C}$ in the $x$-direction can be written as

$$\mathbf{C}(\mathbf{V}) = \begin{pmatrix}
u^1 & 0 & 0 & 0 & 0 & 0 & 0 & 0 & 0 & 0 & 0 & 0 \\
\frac{\rho_1}{\alpha_1}\vartheta_2^1 & u_1^1 & 0 & \rho_1 & 0 & 0 & 0 & 0 & 0 & 0 & 0 & 0 \\
\frac{\rho_2}{\alpha_2}\vartheta_1^1 & 0 & u_2^1 & 0 & 0 & 0 & \rho_2 & 0 & 0 & 0 & 0 & 0 \\
\beta & \frac{a_1^2}{\rho_1} & 0 & u_1^1 & \vartheta_{22}^2 & \vartheta_{22}^3 & 0 & \vartheta_{12}^2 & \vartheta_{12}^3 & 0 & 0 & 0 \\
0 & 0 & 0 & 0 & \xi_2 & 0 & 0 & -\vartheta_{12}^1 & 0 & 0 & 0 & -c_2 a_\psi \\
0 & 0 & 0 & 0 & 0 & \xi_2 & 0 & 0 & -\vartheta_{12}^1 & 0 & c_2 a_\psi & 0 \\
\beta & 0 & \frac{a_2^2}{\rho_2} & 0 & -\vartheta_{12}^2 & -\vartheta_{12}^3 & u_2^1 & -\vartheta_{11}^2 & -\vartheta_{11}^3 & 0 & 0 & 0 \\
0 & 0 & 0 & 0 & \vartheta_{12}^1 & 0 & 0 & \xi_1 & 0 & 0 & 0 & c_1 a_\psi \\
0 & 0 & 0 & 0 & 0 & \vartheta_{12}^1 & 0 & 0 & \xi_1 & 0 & -c_1 a_\psi & 0 \\
0 & 0 & 0 & 0 & 0 & 0 & 0 & 0 & 0 & u^1 & 0 & 0 \\
0 & 0 & 0 & 0 & 0 & a_\psi & 0 & 0 & -a_\psi & 0 & u^1 & 0 \\
0 & 0 & 0 & 0 & -a_\psi & 0 & 0 & a_\psi & 0 & 0 & 0 & u^1
\end{pmatrix},$$

where, as in the previous case, we make use of the auxiliary variables (11) to ease the notation of the matrix. In this case, it is easy to compute the 12 eigenvalues of the matrix $\mathbf{C}$ that are given by

$$\lambda_1 = u_1^1 - a_1, \quad \lambda_2 = u_1^1 + a_1, \quad \lambda_3 = u_2^1 - a_2, \quad \lambda_4 = u_2^1 + a_2,$$
$$\lambda_{5-8} = u^1, \quad \lambda_{9-10} = u^1 - a_\psi, \quad \lambda_{11-12} = u^1 + a_\psi$$

with $a_j$ the sound speed of phase $j$, that is defined as $a_j^2 = \rho_j \left( \frac{\partial h_j}{\partial \rho_j} \right)$, $j = 1, 2$. Since the eigenvalues are real, to check if the system is weakly or strongly hyperbolic, it is necessary to compute the associated eigenvectors. Below, we will write the matrix that contains the right eigenvectors in columns. They are listed in the same order as the eigenvalues

$$\mathbf{R}_{1-8} = \begin{pmatrix} 0 & 0 & 0 & 0 & 0 & \frac{\alpha_1\alpha_2\vartheta_1^3}{\eta_2} & \frac{\alpha_1\alpha_2\vartheta_1^2}{\eta_2} & -\frac{\alpha_1\alpha_2 Z_2}{\eta_2\vartheta_1^1} \\ -\frac{\rho_1}{a_1} & \frac{\rho_1}{a_1} & 0 & 0 & 0 & -\frac{\rho\vartheta_1^3}{\eta_2 Z_1} & -\frac{\rho\vartheta_1^2}{\eta_2 Z_1} & \frac{\zeta_1\rho_1 Z_2}{\eta_2\vartheta_1^1 Z_1} \\ 0 & 0 & -\frac{\rho_2}{a_2} & \frac{\rho_2}{a_2} & 0 & \frac{\alpha_1\rho_2\vartheta_1^3}{\eta_2} & \frac{\alpha_1\rho_2\vartheta_1^2}{\eta_2} & \frac{\zeta_2\rho_2}{\eta_2\vartheta_1^1} \\ 1 & 1 & 0 & 0 & 0 & -\frac{\varepsilon\vartheta_2^1\vartheta_1^3}{\eta_2 Z_1} & -\frac{\varepsilon\vartheta_1^2\vartheta_2^1}{\eta_2 Z_1} & -\frac{c_2\eta_1 Z_2}{c_1\eta_2 Z_1} \\ 0 & 0 & 0 & 0 & 0 & 0 & 1 & 0 \\ 0 & 0 & 0 & 0 & 0 & 1 & 0 & 0 \\ 0 & 0 & 1 & 1 & 0 & 0 & 0 & 1 \\ 0 & 0 & 0 & 0 & 0 & 0 & 1 & 0 \\ 0 & 0 & 0 & 0 & 0 & 1 & 0 & 0 \\ 0 & 0 & 0 & 0 & 1 & 0 & 0 & 0 \\ 0 & 0 & 0 & 0 & 0 & 0 & 0 & 0 \\ 0 & 0 & 0 & 0 & 0 & 0 & 0 & 0 \end{pmatrix},$$

$$\mathbf{R}_{9-12} = \begin{pmatrix} 0 & 0 & 0 & 0 \\ -\frac{\rho_1\tau_2^+\vartheta_2^2}{a_\psi\chi_2^+} & \frac{\rho_1\tau_2^+\vartheta_2^3}{a_\psi\chi_2^+} & \frac{\rho_1\tau_2^-\vartheta_2^2}{a_\psi\chi_2^-} & -\frac{\rho_1\tau_2^-\vartheta_2^3}{a_\psi\chi_2^-} \\ \frac{\rho_2\tau_2^+\vartheta_1^2}{a_\psi\chi_1^-} & -\frac{\rho_2\tau_2^+\vartheta_1^3}{a_\psi\chi_1^-} & -\frac{\rho_2\tau_2^-\vartheta_1^2}{a_\psi\chi_1^+} & \frac{\rho_2\tau_2^-\vartheta_1^3}{a_\psi\chi_1^+} \\ \frac{\delta_2^+\tau_2^+\vartheta_2^2}{a_\psi\chi_2^+} & -\frac{\delta_2^+\tau_2^+\vartheta_2^3}{a_\psi\chi_2^+} & \frac{\delta_2^-\tau_2^-\vartheta_2^2}{a_\psi\chi_2^-} & -\frac{\delta_2^-\tau_2^-\vartheta_2^3}{a_\psi\chi_2^-} \\ \frac{\upsilon_1^-}{a_\psi} & 0 & -\frac{\upsilon_1^+}{a_\psi} & 0 \\ 0 & -\frac{\upsilon_1^-}{a_\psi} & 0 & \frac{\upsilon_1^+}{a_\psi} \\ \frac{\delta_1^-\tau_1^-\vartheta_1^2}{a_\psi\chi_1^-} & -\frac{\delta_1^-\tau_1^-\vartheta_1^3}{a_\psi\chi_1^-} & \frac{\delta_1^+\tau_1^+\vartheta_1^2}{a_\psi\chi_1^+} & -\frac{\delta_1^+\tau_1^+\vartheta_1^3}{a_\psi\chi_1^+} \\ -\frac{\upsilon_2^+}{a_\psi} & 0 & \frac{\upsilon_2^-}{a_\psi} & 0 \\ 0 & \frac{\upsilon_2^+}{a_\psi} & 0 & -\frac{\upsilon_2^-}{a_\psi} \\ 0 & 0 & 0 & 0 \\ 0 & 1 & 0 & 1 \\ 1 & 0 & 1 & 0 \end{pmatrix},$$

where the auxiliary variables that have been used to write the 12 right eigenvectors more compactly are defined as

$$\begin{cases} Z_1 = a_1^2 - (\vartheta_2^1)^2, \quad Z_2 = a_2^2 - (\vartheta_1^1)^2, \quad \eta_1 = \alpha_2(a_1^2 - \alpha_1\beta), \quad \eta_2 = \alpha_1(a_2^2 + \alpha_2\beta), \\ \beta = \dfrac{p_1 - p_2}{\rho}, \quad \vartheta_j^i = c_j w^i, \quad \vartheta_{jk}^i = c_j c_k w^i, \quad \xi_1 = u_2^1 + c_1\vartheta_1^1, \quad \xi_2 = u_1^1 - c_2\vartheta_2^1, \\ \delta_j^\pm = a_\psi \pm \vartheta_j^1, \quad \chi_1^\pm = (\delta_1^\pm)^2 - a_2^2, \quad \chi_2^\pm = (\delta_2^\pm)^2 - a_1^2, \\ \upsilon_1^\pm = c_2\delta_1^\pm, \quad \upsilon_2^\pm = c_1\delta_2^\pm, \quad \tau_1^\pm = \upsilon_1^\pm - c_1 a_\psi, \quad \tau_2^\pm = \upsilon_2^\pm - c_2 a_\psi, \\ \varrho = \alpha_2\big(p_1 + p_2(\gamma_2 - 1) - \rho_1(\vartheta_2^1)^2\big), \quad \varepsilon = \dfrac{\alpha_2}{\rho_1}\big(p_1(\gamma_1 - 1) - p_2(\gamma_2 - 1)\big). \end{cases}$$

Using the GLM curl-cleaning technique, we obtain 12 real eigenvalues and the corresponding 12 linearly independent right eigenvectors, and hence, the augmented system with GLM curl-cleaning (12) is *strongly hyperbolic*.

**2.2.2.2 Symmetrizing Godunov-Powell Terms** The second strategy used to recover the strong hyperbolicity of system (1) is based on the theory of SHTC systems and consists in adding terms that are proportional to the curl involution to the momentum equation (1d), so that the system has real eigenvalues and a complete set of linearly independent eigenvectors, see [16]. The modified system reads

$$\begin{cases} \dfrac{\partial \rho\alpha_1}{\partial t} + \dfrac{\partial \rho\alpha_1 u^k}{\partial x_k} = 0, & (13a)\\ \dfrac{\partial \rho c_1}{\partial t} + \dfrac{\partial (\rho c_1 u^k + \rho E_{w^k})}{\partial x_k} = 0, & (13b)\\ \dfrac{\partial \rho}{\partial t} + \dfrac{\partial \rho u^k}{\partial x_k} = 0, & (13c)\\ \dfrac{\partial \rho u^i}{\partial t} + \dfrac{\partial (\rho u^i u^k + p\delta_{ik} + \rho w^i E_{w^k})}{\partial x_k} + \rho E_{w^k}\left(\dfrac{\partial w^k}{\partial x_i} - \dfrac{\partial w^i}{\partial x_k}\right) = 0, & (13d)\\ \dfrac{\partial w^k}{\partial t} + \dfrac{\partial (w^l u^l + E_{c_1})}{\partial x_k} + u^l\left(\dfrac{\partial w^k}{\partial x_l} - \dfrac{\partial w^l}{\partial x_k}\right) = 0. & (13e) \end{cases}$$

Using (2), system (13) results in

$$\begin{cases} \dfrac{\partial \alpha_1}{\partial t} + u^k \dfrac{\partial \alpha_1}{\partial x_k} = 0, & (14a)\\ \dfrac{\partial \alpha_1\rho_1}{\partial t} + \dfrac{\partial (\alpha_1\rho_1 u_1^k)}{\partial x_k} = 0, & (14b)\\ \dfrac{\partial \alpha_2\rho_2}{\partial t} + \dfrac{\partial (\alpha_2\rho_2 u_2^k)}{\partial x_k} = 0, & (14c)\\ \dfrac{\partial \rho u^i}{\partial t} + \dfrac{\partial (\alpha_1\rho_1 u_1^i u_1^k + \alpha_2\rho_2 u_2^i u_2^k + p\delta_{ik})}{\partial x_k} + \rho c_1 c_2 w^k\left(\dfrac{\partial w^k}{\partial x_i} - \dfrac{\partial w^i}{\partial x_k}\right) = 0, & (14d)\\ \dfrac{\partial w^k}{\partial t} + \dfrac{\partial}{\partial x_k}\left(\dfrac{1}{2}(u_1^l)^2 - \dfrac{1}{2}(u_2^l)^2 + h_1 - h_2\right) + u^l\left(\dfrac{\partial w^k}{\partial x_l} - \dfrac{\partial w^l}{\partial x_k}\right) = 0. & (14e) \end{cases}$$

As in the previous case, the eigenvalues and eigenvectors are computed to analyze the hyperbolicity of the system (14). The matrix $\mathbf{C}$ in the $x$-direction reads as

$$\mathbf{C}(\mathbf{V}) = \begin{pmatrix} u^1 & 0 & 0 & 0 & 0 & 0 & 0 & 0 & 0 \\ \frac{\rho_1}{\alpha_1}\vartheta_2^1 & u_1^1 & 0 & \rho_1 & 0 & 0 & 0 & 0 & 0 \\ \frac{\rho_2}{\alpha_2}\vartheta_1^1 & 0 & u_2^1 & 0 & 0 & 0 & \rho_2 & 0 & 0 \\ \beta & \frac{a_1^2}{\rho_1} & 0 & u_1^1 & \vartheta_2^2 & \vartheta_2^3 & 0 & 0 & 0 \\ 0 & 0 & 0 & 0 & u^1 & 0 & 0 & 0 & 0 \\ 0 & 0 & 0 & 0 & 0 & u^1 & 0 & 0 & 0 \\ \beta & 0 & \frac{a_2^2}{\rho_2} & 0 & 0 & 0 & u_2^1 & -\vartheta_1^2 & -\vartheta_1^3 \\ 0 & 0 & 0 & 0 & 0 & 0 & 0 & u^1 & 0 \\ 0 & 0 & 0 & 0 & 0 & 0 & 0 & 0 & u^1 \end{pmatrix}.$$

As previously, we have used the auxiliary variables (11) to lighten the matrix. In this case, the nine eigenvalues of the matrix $\mathbf{C}$ are given by

$$\lambda_1 = u_1^1 - a_1, \quad \lambda_2 = u_1^1 + a_1, \quad \lambda_3 = u_2^1 - a_2, \quad \lambda_4 = u_2^1 + a_2, \quad \lambda_{5-9} = u^1$$

with $a_j$ the sound speed of phase $j$, which is defined as $a_j^2 = \rho_j\left(\frac{\partial h_j}{\partial \rho_j}\right)$, $j = 1, 2$. Since the eigenvalues are all real, to check if the system is weakly or strongly hyperbolic, it is necessary to compute the associated eigenvectors. Below, we will write the matrix that contains the right eigenvectors in columns. They are listed in the same order as the eigenvalues

$$\mathbf{R} = \begin{pmatrix} 0 & 0 & 0 & 0 & \frac{\alpha_1\alpha_2\vartheta_1^3}{\eta_2} & \frac{\alpha_1\alpha_2\vartheta_1^2}{\eta_2} & -\frac{\alpha_1\alpha_2 Z_2}{\eta_2\vartheta_1^1} & 0 & 0 \\ \frac{-\rho_1}{a_1} & \frac{\rho_1}{a_1} & 0 & 0 & -\frac{\zeta_1\rho_1\vartheta_1^3}{\eta_2 Z_1} & -\frac{\zeta_1\rho_1\vartheta_1^2}{\eta_2 Z_1} & \frac{\zeta_1\rho_1 Z_2}{\eta_2\vartheta_1^1 Z_1} & -\frac{\rho_1\vartheta_2^3}{Z_1} & -\frac{\rho_1\vartheta_2^2}{Z_1} \\ 0 & 0 & \frac{-\rho_2}{a_2} & \frac{\rho_2}{a_2} & \frac{\alpha_1\rho_2\vartheta_1^3}{\eta_2} & \frac{\alpha_1\rho_2\vartheta_1^2}{\eta_2} & \frac{\zeta_2\rho_2}{\eta_2\vartheta_1^1} & 0 & 0 \\ 1 & 1 & 0 & 0 & \frac{\eta_1\vartheta_2^1\vartheta_1^3}{\eta_2 Z_1} & \frac{\eta_1\vartheta_2^1\vartheta_1^2}{\eta_2 Z_1} & -\frac{c_2\eta_1 Z_2}{c_1\eta_2 Z_1} & \frac{\vartheta_2^1\vartheta_2^3}{Z_1} & \frac{\vartheta_2^1\vartheta_2^2}{Z_1} \\ 0 & 0 & 0 & 0 & 0 & 0 & 0 & 0 & 1 \\ 0 & 0 & 0 & 0 & 0 & 0 & 0 & 1 & 0 \\ 0 & 0 & 1 & 1 & 0 & 0 & 1 & 0 & 0 \\ 0 & 0 & 0 & 0 & 0 & 1 & 0 & 0 & 0 \\ 0 & 0 & 0 & 0 & 1 & 0 & 0 & 0 & 0 \end{pmatrix},$$

where the auxiliary variables used to write the nine right eigenvectors more compactly are defined as

$$Z_1 = a_1^2 - (\vartheta_2^1)^2, \quad Z_2 = a_2^2 - (\vartheta_1^1)^2, \quad \eta_1 = \alpha_2(a_1^2 - \alpha_1\beta),$$
$$\eta_2 = \alpha_1(a_2^2 + \alpha_2\beta), \quad \zeta_1 = \alpha_2\left(\alpha_1\beta - (\vartheta_2^1)^2\right), \quad \zeta_2 = \alpha_1\left(\alpha_2\beta + (\vartheta_1^1)^2\right).$$

Since we have obtained nine real eigenvalues with a full set of linearly independent eigenvectors, the system (14) with the additional symmetrizing Godunov-Powell terms is strongly hyperbolic.

## 3 High-Order ADER-DG Finite-Element Scheme with *a posteriori* Subcell Finite-Volume Limiter

As described in Sect. 2 and Refs. [59, 62, 69], the system (4) is a hyperbolic system that can be compactly written as

$$\frac{\partial \mathbf{Q}}{\partial t} + \nabla \cdot \mathbf{F}(\mathbf{Q}) + \mathbf{B}(\mathbf{Q}) \cdot \nabla \mathbf{Q} = \mathbf{S}(\mathbf{Q}), \tag{15}$$

where $\mathbf{Q}$ is the vector of conserved variables, $\mathbf{F} = (\mathbf{f}, \mathbf{g}, \mathbf{h})$ is the flux tensor, $\mathbf{B}(\mathbf{Q}) \cdot \nabla \mathbf{Q} = \mathbf{B}_1(\mathbf{Q})\frac{\partial}{\partial x}\mathbf{Q} + \mathbf{B}_2(\mathbf{Q})\frac{\partial}{\partial y}\mathbf{Q} + \mathbf{B}_3(\mathbf{Q})\frac{\partial}{\partial z}\mathbf{Q}$ are the non-conservative terms, and $\mathbf{S}$ is the vector of algebraic source terms. To solve the system (15), we will use high-order ADER-DG schemes with *a posteriori* subcell finite-volume limiter on uniform Cartesian meshes, see [24, 26, 27, 33, 34, 76] for further details. In this work, for the time-evolution, we propose to use a local space-time DG predictor, instead of using the Cauchy-Kovalevskaya procedure, following [27, 28]. The main reasons for this choice are the following: compared to the Cauchy-Kovalevskaya procedure, which is rather cumbersome, the local space-time DG predictor is much more general and simpler to implement for complex hyperbolic PDE systems as the ones studied in this paper. Furthermore, it allows also to deal with stiff source terms, like stiff velocity and pressure relaxation terms.

### 3.1 One-Step ADER-DG Schemes

In the following, a description of the method is given for the two-dimensional (2D) case ($d = 2$). The computational domain $\Omega = [-L_x/2, L_x/2] \times [-L_y/2, L_y/2]$ is discretized with a Cartesian grid composed of $N_x \times N_y$ cells. These cells are given by $\Omega_i = [x_i - \frac{\Delta x}{2}, x_i + \frac{\Delta x}{2}] \times [y_i - \frac{\Delta x}{2}, y_i + \frac{\Delta y}{2}]$ with $(x_i, y_i)$ the barycenter of the cell $\Omega_i$, and $\Delta x = \frac{L_x}{N_x}$, $\Delta y = \frac{L_y}{N_y}$ the mesh spacing in the $x$- and $y$-directions. Let $\boldsymbol{u}_h(\mathbf{x}, t^n)$ be the discrete solution of (15) in each spatial control volume $\Omega_i$ at time $t^n$, written in terms of tensor products of piecewise polynomials of degree $N$, and let $V_h$ be the space of tensor products of piecewise polynomials of the degree up to $N$. Then, the discrete solution $\boldsymbol{u}_h$ can be written in terms of the basis functions, $\varphi_l(x, y)$, $l \in [1, (N+1)^d]$, in every cell $\Omega_i$ as

$$\boldsymbol{u}_h(\mathbf{x}, t^n) = \varphi_l(\mathbf{x})\hat{\boldsymbol{u}}_l^n, \quad \mathbf{x} \in \Omega_i, \tag{16}$$

where $\varphi_l = \varphi_l(\mathbf{x})$ are the basis functions associated with $V_h$. We take an orthogonal nodal basis $\{\varphi_l\}_{l \in \{0,\cdots,(N+1)^d\}}$, generated by the tensor product $\{\varphi_{l_1}\varphi_{l_2}\varphi_{l_3}\}_{l_1,l_2,l_3 \in \{0,\cdots,N\}}$, where $\{\varphi_{l_i}\}_{l_i \in \{0,\cdots,N\}}$ are the Lagrange interpolation polynomials going through the $N+1$ Gauss-Legendre quadrature nodes. Multiplying (15) by a test function $\varphi_l \in V_h$, and integrating the equation over the space-time control volume $\Omega_i \times [t^n, t^{n+1}]$, the weak formulation can be written as

$$\int_{t^n}^{t^{n+1}} \int_{\Omega_i} \left( \frac{\partial \mathbf{Q}}{\partial t} + \nabla \cdot \mathbf{F}(\mathbf{Q}) + \mathbf{B}(\mathbf{Q}) \cdot \nabla \mathbf{Q} \right) \varphi_l \, \mathrm{d}\mathbf{x}\mathrm{d}t = \int_{t^n}^{t^{n+1}} \int_{\Omega_i} \mathbf{S}(\mathbf{Q})\varphi_l \, \mathrm{d}\mathbf{x}\mathrm{d}t. \tag{17}$$

To achieve high order in space and time, an ADER approach can be used. This methodology was put forward by Toro et al. for the first time in [72] for linear problems on Cartesian

meshes, it can be implemented in both the finite volume and the DG finite-element framework and is uniformly and arbitrarily high-order accurate in both space and time. In this work, an alternative version of the ADER approach is considered, avoiding the use of the Cauchy-Kovalevskaya procedure using a local space-time DG predictor, which is based on a weak space-time formulation of the governing PDE (17).

Using (16) and integrating the term with the time derivative by parts in time and the divergence term by parts in space, then (17) results in

$$\begin{aligned}&\left(\int_{\Omega_i}\varphi_k\varphi_l\,\mathrm{d}\mathbf{x}\right)\left(\hat{\boldsymbol{u}}_{l,i}^{n+1}-\hat{\boldsymbol{u}}_{l,i}^{n}\right)+\int_{t^n}^{t^{n+1}}\int_{\partial\Omega_i}\varphi_k\left(\mathcal{G}\left(\mathbf{q}_h^-,\mathbf{q}_h^+\right)+\mathcal{D}\left(\mathbf{q}_h^-,\mathbf{q}_h^+\right)\right)\cdot\mathbf{n}\,\mathrm{d}S\mathrm{d}t\\&-\int_{t^n}^{t^{n+1}}\int_{\Omega_i}\nabla\varphi_k\cdot\mathbf{F}(\mathbf{q}_h)\,\mathrm{d}\mathbf{x}\mathrm{d}t=\int_{\Omega_i}\varphi_k\mathbf{S}(\mathbf{q}_h)\,\mathrm{d}\mathbf{x}\mathrm{d}t,\end{aligned}\tag{18}$$

where $\mathbf{n}$ is the outward unit normal vector at the cell boundary $\partial\Omega_i$, $\mathbf{q}_h$ is a local space-time predictor, which will be explained below, and $\mathbf{q}_h^+$ and $\mathbf{q}_h^-$ are the boundary-extrapolated values of the space-time predictor from within $\Omega_i$ and its neighbor $\Omega_j$. Usually, $\mathbf{q}_h$ presents jumps across the cell boundaries, which can be resolved by the solution of a generalized Riemann problem (see [40, 71] for more details). In (18), $\mathcal{G}$ denotes the Riemann solver (numerical flux function), which depends on the left state $\mathbf{q}_h^-$ and the right state $\mathbf{q}_h^+$. In this case, this integral has been approximated using the Rusanov flux, see [64]

$$\mathcal{G}(\mathbf{q}_h^-,\mathbf{q}_h^+)\cdot\mathbf{n}=\frac{1}{2}\left(\mathbf{F}(\mathbf{q}_h^+)+\mathbf{F}(\mathbf{q}_h^-)\right)\cdot\mathbf{n}-\frac{1}{2}s_{\max}\mathbf{I}\left(\mathbf{q}_h^+-\mathbf{q}_h^-\right),\tag{19}$$

where $s_{\max}=\max\left(\left|\lambda_k(\mathbf{q}_h^+)\right|,\left|\lambda_k(\mathbf{q}_h^-)\right|\right)$ is the maximum wave speed at the interface. To deal with the jump terms in the non-conservative product, a path-conservative method is employed, following [13, 51]. In this setting, a straight-line segment path is chosen

$$\Psi(s,\mathbf{q}_h^+,\mathbf{q}_h^-)=\mathbf{q}_h^-+s(\mathbf{q}_h^+-\mathbf{q}_h^+),\quad s\in[0,1],$$

so that the non-conservative terms reduce to the following expression:

$$\mathcal{D}(\mathbf{q}_h^-,\mathbf{q}_h^+)\cdot\mathbf{n}=\frac{1}{2}\widetilde{\mathbf{B}}\cdot(\mathbf{q}_h^+-\mathbf{q}_h^-)\quad\text{with}\quad\widetilde{\mathbf{B}}=\int_0^1\mathbf{B}(\Psi(s,\mathbf{q}_h^+,\mathbf{q}_h^-))\cdot\mathbf{n}\,\mathrm{d}S.$$

### 3.2 Local Space-Time Predictor

In the following, we describe the local space-time predictor used to compute the coefficients $\hat{\boldsymbol{u}}_{l,i}^n$ in Eq. (18). We consider space-time basis functions $\theta_l$, that are obtained as the tensor product $\theta_l(\mathbf{x},t)=\varphi_{k_0}(t)\varphi_{k_1}(\mathbf{x})$, of the same previously introduced Lagrange interpolation polynomials, just that now the basis functions also depend on time. The predictor $\mathbf{q}_h$ is written in the form

$$\mathbf{q}_h(\mathbf{x},t)=\theta_l(\mathbf{x},t)\hat{\mathbf{q}}_{l,i}\tag{20}$$

as a weak solution to (15). Then, using (20) in (15), multiplying by a space-time basis function $\theta_l$ and integrating over $\Omega_i\times[t^n,t^{n+1}]$ yields

$$\int_{t^n}^{t^{n+1}} \int_{\Omega_i} \theta_l \big( \boldsymbol{U}_t + \nabla \cdot \mathbf{F}(\boldsymbol{U}) + \mathbf{B}(\boldsymbol{U}) \cdot \nabla \boldsymbol{U} \big) \mathrm{d}\mathbf{x}\mathrm{d}t = \int_{t^n}^{t^{n+1}} \int_{\Omega_i} \theta_l (\mathbf{S}(\boldsymbol{U})) \mathrm{d}\mathbf{x}\mathrm{d}t.$$

Integrating by parts only the first term on the left-hand side and taking into account that at time $t^n$, we start from the known state $\boldsymbol{u}_h^n$ allows us to write

$$\begin{aligned} &\int_{\Omega_i} \theta_l(\mathbf{x}, t^{n+1}) \mathbf{q}_h(\mathbf{x}, t^{n+1}) \, \mathrm{d}\mathbf{x} - \int_{\Omega_i} \theta_l(\mathbf{x}, t^n) \boldsymbol{u}_h(\mathbf{x}, t^n) \, \mathrm{d}\mathbf{x} - \int_{t^n}^{t^{n+1}} \int_{\Omega_i} \frac{\partial \theta_l}{\partial t} \mathbf{q}_h \, \mathrm{d}\mathbf{x}\mathrm{d}t \\ &+ \int_{t^n}^{t^{n+1}} \int_{\Omega_i} \theta_l \nabla \cdot \mathbf{F}(\mathbf{q}_h) \, \mathrm{d}\mathbf{x}\mathrm{d}t + \int_{t^n}^{t^{n+1}} \int_{\Omega_i^\circ} \theta_l \mathbf{B}(\mathbf{q}_h) \cdot \nabla \mathbf{q}_h \, \mathrm{d}\mathbf{x}\mathrm{d}t = \int_{t^n}^{t^{n+1}} \int_{\Omega_i} \theta_l \mathbf{S}(\mathbf{q}_h) \, \mathrm{d}\mathbf{x}\mathrm{d}t \end{aligned} \tag{21}$$

with $\Omega_i^\circ = \frac{\Omega_i}{\partial \Omega_i}$. Equation (21) is a system for the unknowns $\hat{\mathbf{q}}$ of the space-time predictor $\mathbf{q}_h(\mathbf{x}, t)$ and can be computed in terms of the spatial degrees of freedom $\hat{\boldsymbol{u}}_l^n$. It is solved by a fixed point iteration for which convergence was proven in [10]. Once the predictor is known, Eq. (18) allows to compute the polynomial coefficients $\hat{\boldsymbol{u}}^{n+1}$ in each cell using Gaussian quadrature for the remaining integrals.

### 3.3 *A Posteriori* Subcell Finite-Volume Limiter

Although the numerical method presented in the previous section is a high-order method, it is linear in the sense of Godunov, which means that spurious oscillations will appear in the presence of discontinuities or shock waves. To overcome this problem, we use the *a posteriori* subcell limiter for high-order fully discrete one-step ADER-DG schemes presented in [34, 76]. This subcell finite-volume limiter is based on the MOOD paradigm introduced in [17, 22, 23] for finite-volume schemes.

The scheme described in the previous section is run over the entire domain at each time step, and a so-called candidate solution $\boldsymbol{u}_h^*(\mathbf{x}, t^{n+1})$ is obtained. Then, one checks whether the candidate solution verifies some numerical and physical detection criteria (positivity of the densities $\rho_1$ and $\rho_2$, $\alpha_1$ with values between 0 and 1) and whether the discrete maximum principle (DMP), [34], is verified. If a cell $\Omega_i$ violates any of the above criteria, that cell is flagged as a troubled cell and for the application of the subcell finite-volume limiter. The limiter is denoted as *a posteriori*, because it is applied after the candidate solution has been computed.

The limiter is applied in the following way: all cells $\Omega_i$ marked as troubled are subdivided into $(2N+1)^d$ subcells, which are denoted by $\Omega_{i,j}$ where $\Omega_i = \bigcup_j \Omega_{i,j}$. The discrete solution at time $t^n$ is given by the piecewise constant cell averages, denoted by $\bar{\boldsymbol{u}}_{i,j}^n$. They are obtained from the high-order DG polynomials $\boldsymbol{u}_h(\mathbf{x}, t^n)$ by averaging using the definition of the cell average

$$\bar{\boldsymbol{u}}_{i,j}^n = \frac{1}{|\Omega_{i,j}|} \int_{\Omega_{i,j}} \boldsymbol{u}_h(\mathbf{x}, t^n) \, \mathrm{d}\mathbf{x}. \tag{22}$$

It is worth noting that subdividing a high-order DG element into $2N+1$ finite-volume subcells per space dimension does *not* reduce the time step size of the overall scheme, since the CFL stability condition of explicit DG schemes scales with $1/(2N+1)$ in one dimension, while the maximum Courant number of finite-volume methods is unity in one space dimension.

The cell averages (22) are evolved in time using either a second-order MUSCL-Hancock-type TVD finite-volume scheme with the minmod limiter, or by making use of a third-order ADER-WENO finite-volume scheme, see [34], which are also both predictor-corrector methods, and thus look almost identical to the ADER-DG scheme, except for the necessary nonlinear reconstruction step. Moreover, in this case, the test function is unity, which implies that the volume integral over the flux term disappears and the volumes computed over $\Omega_i$ are replaced by the volumes over the subcells $\Omega_{i,j}$, and hence

$$\begin{aligned} &\left|\Omega_{i,j}\right|\left(\bar{\boldsymbol{u}}_{i,j}^{n+1}-\bar{\boldsymbol{u}}_{i,j}^{n}\right)+\int_{t^n}^{t^{n+1}}\int_{\partial\Omega_{i,j}}\left(\mathcal{G}\left(\mathbf{q}_h^-,\mathbf{q}_h^+\right)+\mathcal{D}\left(\mathbf{q}_h^-,\mathbf{q}_h^+\right)\right)\cdot\mathbf{n}\,\mathrm{d}S\mathrm{d}t \\ &+\int_{t^n}^{t^{n+1}}\int_{\Omega_{i,j}^{\circ}}\left(\mathbf{B}(\mathbf{q}_h)\cdot\nabla\mathbf{q}_h\right)\mathrm{d}\mathbf{x}\mathrm{d}t=\int_{t^n}^{t^{n+1}}\int_{\Omega_{i,j}}\mathbf{S}(\mathbf{q}_h,\nabla\mathbf{q}_h)\mathrm{d}\mathbf{x}\mathrm{d}t\,. \end{aligned} \tag{23}$$

The limited DG polynomial $\boldsymbol{u}_h'$ at time $t^{n+1}$ is then obtained by performing a constrained least-squares reconstruction and using the averages of all the subcells of $\Omega_i$ computed using (23). The reconstruction reads

$$\frac{1}{|\Omega_{i,j}|}\int_{\Omega_{i,j}}\boldsymbol{u}_h'(\mathbf{x},t^{n+1})\mathrm{d}\mathbf{x}=\bar{\boldsymbol{u}}_{i,j}^{n+1},\quad\forall\,\Omega_{i,j}\in\Omega_i$$

with the linear constraint

$$\int_{\Omega_i}\boldsymbol{u}_h'(\mathbf{x},t^{n+1})\mathrm{d}\mathbf{x}=\sum_{\Omega_{i,j}\in\Omega_i}|\Omega_{i,j}|\bar{\boldsymbol{u}}_{i,j}^{n+1}. \tag{24}$$

The constraint (24) means conservation of the solution within the element $\Omega_i$. In addition to the expansion coefficients $\hat{\boldsymbol{u}}_{i,l}^{n+1}$ of the limited DG polynomial, in all limited DG elements, we also keep in memory the averages of the finite-volume subcells $\bar{\boldsymbol{u}}_{i,j}^{n+1}$, as they serve as the initial condition for the finite-volume limiter of the subcell in case a cell is problematic also in the next time step, see [34]. More details about the *a posteriori* subcell finite-volume limiter can be found in [31, 34, 76].

## 4 Numerical Results

This section is devoted to showing some test cases to illustrate the high order of the accuracy of the proposed method, especially in the presence of steep gradients in the solution. First, some simulations are performed to show the experimental order of convergence (EOC) of the proposed ADER-DG method. Then, our scheme is used to solve some Riemann problems in one and two dimensions. Finally, a dambreak problem is simulated, and the results are compared with those obtained with a reduced BN model. Although the original system is only weakly hyperbolic, no stability problems have been found in the numerical simulations, contrary to what was reported in [15, 16, 21] for other weakly hyperbolic systems with curl involutions. In this section, some test cases are performed considering the original system (4), and some others, such as the convergence analysis and the dambreak, are solved using not only the original system but also the new GLM curl-cleaning technique and the symmetrizing Godunov-Powell terms to compare the solutions. Moreover, in all tests, the algebraic relaxation source terms have been neglected,

and the gravity $\boldsymbol{g}$ is set to $\mathbf{0}$, except in the dambreak test case, where it is necessary to consider the gravity.

### 4.1 Accuracy Analysis

This section performs a numerical convergence analysis to show the EOC of the proposed ADER-DG method. To construct an exact solution, following [5, 30], an analytical, stationary, and rotationally symmetric solution of the system (4) is computed considering cylindrical coordinates ($r$, $\theta$, and $z$) with $(u^r, u^\theta, u^z)$ the velocity vector and $(w^r, w^\theta, w^z)$ the relative velocity vector. The analytical solution is assumed to approach a constant state as the radial coordinate $r$ tends to infinity to be compatible with periodic boundary conditions.

To obtain a steady analytical solution, we first write an equivalent PDE system in the radial direction. For this purpose, the pressure and the velocity relaxation are neglected, the gravity is set to zero, and system (4) is rewritten in cylindrical coordinates and assuming no variations in the $z$-direction ($\frac{\partial}{\partial z} = 0$) and considering rotational symmetry ($\frac{\partial}{\partial \theta} = 0$). The resulting system in radial direction reads

$$
\begin{cases}
\dfrac{\partial \alpha_1}{\partial t} + u^r \dfrac{\partial \alpha_1}{\partial r} = 0, & \text{(25a)} \\[2ex]
\dfrac{\partial \alpha_1 \rho_1}{\partial t} + \dfrac{1}{r} \dfrac{\partial (r \alpha_1 \rho_1 u_1^r)}{\partial r} = 0, & \text{(25b)} \\[2ex]
\dfrac{\partial \alpha_2 \rho_2}{\partial t} + \dfrac{1}{r} \dfrac{\partial (r \alpha_2 \rho_2 u_2^r)}{\partial r} = 0, & \text{(25c)} \\[2ex]
\dfrac{\partial \rho u^r}{\partial t} + \dfrac{\partial (\alpha_1 \rho_1 (u_1^r)^2 + \alpha_2 \rho_2 (u_2^r)^2 + p)}{\partial r} + \alpha_1 \rho_1 \dfrac{(u_1^r)^2 - (u_1^\theta)^2}{r} + \alpha_2 \rho_2 \dfrac{(u_2^r)^2 - (u_2^\theta)^2}{r} = 0, & \text{(25d)} \\[2ex]
\dfrac{\partial \rho u^\theta}{\partial t} + \dfrac{\partial (\alpha_1 \rho_1 u_1^r u_1^\theta + \alpha_2 \rho_2 u_2^r u_2^\theta)}{\partial r} + 2 \dfrac{\alpha_1 \rho_1 u_1^r u_1^\theta + \alpha_2 \rho_2 u_2^r u_2^\theta}{r} = 0, & \text{(25e)} \\[2ex]
\dfrac{\partial w^r}{\partial t} + \dfrac{\partial}{\partial r} \left( \dfrac{1}{2} (u_1^l)^2 - \dfrac{1}{2} (u_2^l)^2 + h_1 - h_2 \right) = 0, & \text{(25f)} \\[2ex]
\dfrac{\partial w^\theta}{\partial t} = 0, & \text{(25g)}
\end{cases}
$$

where the constraint $\nabla \times \boldsymbol{w} = 0$ has been used in the last two equations. Since we are looking for a vortex-type solution, the radial velocities vanish, that is, we set $u^r = u_1^r = u_2^r = w^r = 0$. Also, we are interested in a stationary solution, hence $\partial_t = 0$. With these assumptions, the system (25) reduces to

$$\alpha_1\rho_1\frac{(u_1^\theta)^2}{r}+\alpha_2\rho_2\frac{(u_2^\theta)^2}{r}-\frac{\partial p}{\partial r}=0, \tag{26a}$$

$$\frac{\partial}{\partial r}\left(\frac{1}{2}(u^\theta)^2-\frac{1}{2}(u^\theta)^2+h_1-h_2\right)=0. \tag{26b}$$

With some simple algebra in (26), we get

$$\begin{cases}(u_1^\theta)^2=\dfrac{r}{\rho}\dfrac{\partial p}{\partial r}+2\dfrac{\alpha_2\rho_2}{\rho}(k-h_1+h_2), & \text{(27a)}\\[2ex] (u_2^\theta)^2=\dfrac{r}{\rho}\dfrac{\partial p}{\partial r}-2\dfrac{\alpha_1\rho_1}{\rho}(k-h_1+h_2), & \text{(27b)}\end{cases}$$

where $k$ is a constant. Now, we prescribe radial profiles for $\alpha_1$ and $p_i$ as

$$\alpha_1=\frac{1}{3}+\frac{\mathrm{e}^{-\frac{r^2}{2}}}{2\sqrt{2\pi}},\qquad p_i=1-\frac{\mathrm{e}^{1-r^2}}{4},$$

and then, the densities $\rho_i$ and the velocities $u_i^\theta$ result as

$$\rho_i=\left(1-\frac{\mathrm{e}^{1-r^2}}{4}\right)^{5/7},\qquad u_i^\theta=2^{3/14}\sqrt{\frac{\mathrm{e}^{1-r^2}r^2}{\left(4-\mathrm{e}^{1-r^2}\right)^{5/7}}}.$$

With this, we have computed an exact stationary and rotationally symmetric solution of the PDE system (25) that approaches a constant state as $r\to\infty$ to be compatible with periodic boundary conditions. Figure 1 shows the contours of the volume fraction function for our vortex-type solution together with the velocity but remains stationary due to its symmetry.

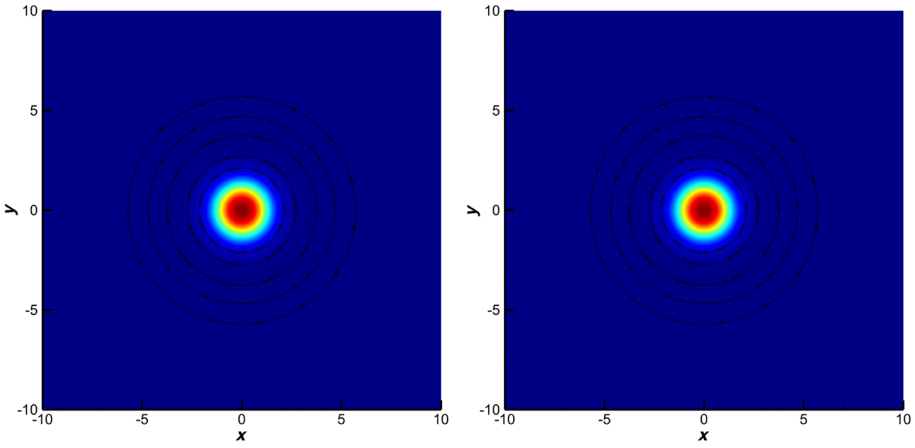


**Fig. 1** $\alpha$ field for the stationary vortex-type solution at times $t=0,\ 1$. The velocity streamlines are plotted to show that the solution is symmetric and is rotating over time

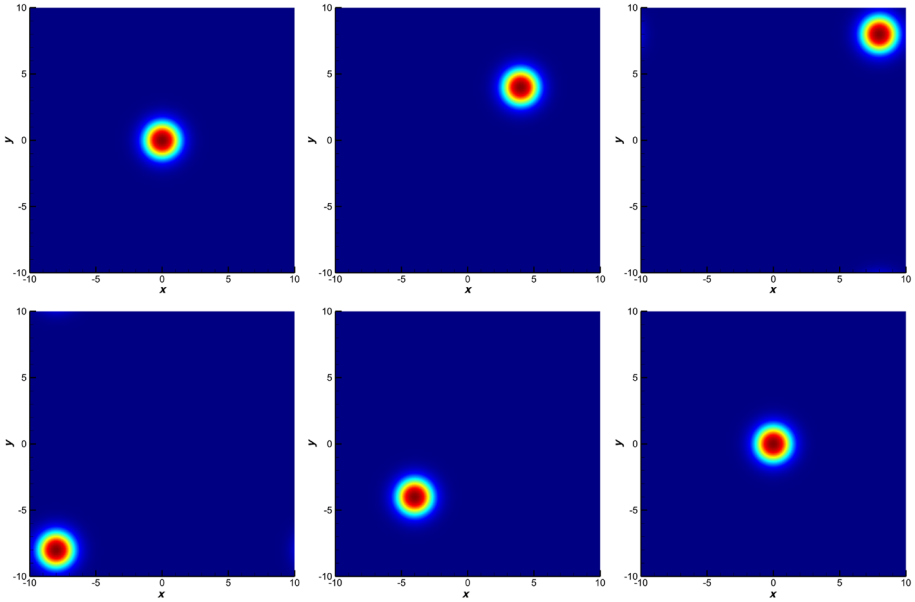

**Fig. 2** Value of $\alpha$ for the unsteady vortex at times $t = 0,\ 1,\ 2,\ 3,\ 4,\ 5$

Then, using the principle of the Galilean invariance, we can make the test unsteady if we add a uniform velocity field to this solution. After one advection period through a periodic computational domain, the exact solution will be given by the initial condition and we can perform the convergence test.

To analyze the convergence order, we compute the solution with the proposed method, using different orders for the DG scheme, and compare it with the exact solution derived above. The computational domain is $\Omega = [-10, 10]^2$ with the final simulation time $t = 1$ and periodic boundary conditions everywhere. Different polynomial approximation degrees have been considered for the DG scheme. The $L^2$ errors and the corresponding numerical convergence rates for $N = 2, 3, 4, 5$ are given in Table 1, showing the expected order of convergence.

For analyzing the convergence order using the unsteady solution, we make use of the principle of the Galilean invariance of Newtonian mechanics. We add a constant uniform velocity field $\bar{u}_1 = \bar{u}_2 = 4$ to both phases. The computational domain is the same as before $\Omega = [-10, 10] \times [-10, 10]$ with the final simulation time $t = 5$ and periodic boundary conditions everywhere. Figure 2 shows that this solution is symmetric and rotates over time, as the stationary one, but the vortex is transported with constant velocities $\bar{u}_1 = \bar{u}_2 = 4$. At time $t = 5$, after one advection period, the solution will be the initial one. The $L^2$ errors and the corresponding convergence rates for the different degrees $N = 2, 3, 4, 5$ are given in Table 2, finding the expected convergence order $N + 1$ of our high-order ADER-DG schemes.

Finally, we will perform a convergence analysis with the same unsteady solution used in the previous case, where we can compare the convergence order for the original system, as well as for the systems augmented with the GLM approach with the curl-cleaning speed $a_\psi = 1$ and with the Godunov-Powell terms. Table 3 shows the errors in the $L^2$ norm and

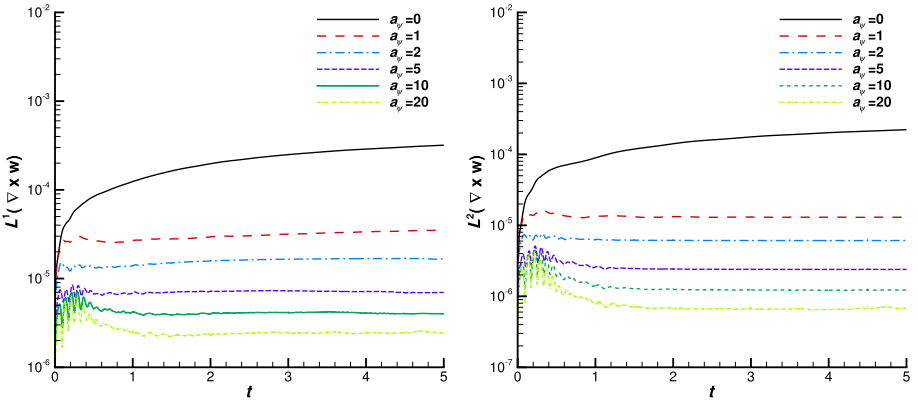


**Fig. 3** Time evolution of the $L^1$ (left) and $L^2$ (right) norms of the curl errors

the convergence orders for $N = 3$. The difference among the errors for the three systems is almost negligible and the order of convergence is four, as expected.

For this test, we have also computed the $L^1$ and $L^2$ norms of the curl errors for different values of $a_\psi$, to illustrate the time-evolution of these errors as a function of $a_\psi$. As we can expected, the curl errors are decreasing when the GLM curl-cleaning speed $a_\psi$ is increasing, as one can see in Fig. 3.

### 4.2 The 1D Riemann Problem

This section is devoted to studying the behavior of the proposed methodology in the presence of shocks. First, we solve one of the 1D Riemann problems proposed in [69], where a shock in one phase appears inside a rarefaction of the other phase. This Riemann problem presents a discontinuity in $x = 0$ and has the left and right states shown in Table 4.

Since the problem that we want to reproduce is a 1D problem, $u^2 = u^3 = 0$ and $w^2 = w^3 = 0$. The computational domain is $\Omega = [-1, 1]$ and has been discretized using a fourth-order ADER-DG scheme ($N = 3$) with *a posteriori* subcell limiter on a mesh with 8 192 cells. The simulation is performed up to $t = 0.25$, and the CFL number is set to 0.25. Two ideal gases are considered for both phases with EOS (6), setting $s_i = 0$, $\gamma_1 = 1.4$, and $\gamma_2 = 2$, respectively. In Fig. 4, the numerical results are shown together with the reference solution computed with a second-order MUSCL-Hancock scheme based on the Rusanov flux as approximate Riemann solver and using a mesh spacing of $\Delta x = 2 \times 10^{-6}$ (see [69] for further details). We observe an excellent agreement between our numerical solution and the reference solution. Looking at the density and velocity of each phase, we see that as long as shock waves are absent, the rarefaction only affects the related phase, but that the interaction of the two rarefactions is observed in the mixing quantities. In addition, in the density of the first phase, we can see that to the right of the contact, a rarefaction begins (which does not affect the second phase) until the shock occurs. Once the shock appears inside the right rarefaction, the density jumps according to the jump conditions. Then, on the right, a plateau of the right state of the shock is observed inside the rarefaction, and then, the rarefaction continues again, see [69] for a detailed discussion of this peculiar shock-in-rarefaction phenomenon, which is a particular

**Table 1** Numerical convergence results for high-order DG schemes of polynomial approximation $N = 2, 3, 4, 5$ with a uniform Cartesian mesh of $N_x \times N_y$ elements. The $L^2$ error norms and the corresponding orders of the convergence of the variables $\alpha_1$, $\rho_1$, $\rho_2$, $u_1$, and $u_2$ are computed at time $t = 1$

| $N = 2$ | | | | | |
|---|---|---|---|---|---|
| $N_x = N_y$ | $L^2_\Omega(\alpha_1)$ | $L^2_\Omega(\rho_1)$ | $L^2_\Omega(\rho_2)$ | $L^2_\Omega(u_1)$ | $L^2_\Omega(u_2)$ |
| 16 | $4.273\,7 \times 10^{-3}$ | $2.590\,7 \times 10^{-2}$ | $2.611\,7 \times 10^{-2}$ | $6.770\,6 \times 10^{-2}$ | $6.405\,8 \times 10^{-2}$ |
| 32 | $1.077\,6 \times 10^{-3}$ | $4.731\,5 \times 10^{-3}$ | $4.474\,6 \times 10^{-3}$ | $1.014\,6 \times 10^{-2}$ | $9.225\,7 \times 10^{-3}$ |
| 64 | $2.138\,0 \times 10^{-4}$ | $6.721\,2 \times 10^{-4}$ | $6.240\,5 \times 10^{-4}$ | $1.647\,9 \times 10^{-3}$ | $1.525\,0 \times 10^{-3}$ |
| 128 | $3.352\,2 \times 10^{-5}$ | $9.523\,7 \times 10^{-5}$ | $8.719\,3 \times 10^{-5}$ | $2.770\,9 \times 10^{-4}$ | $2.611\,6 \times 10^{-4}$ |
| 256 | $4.785\,4 \times 10^{-6}$ | $1.298\,7 \times 10^{-5}$ | $1.164\,5 \times 10^{-5}$ | $4.383\,6 \times 10^{-5}$ | $4.195\,5 \times 10^{-5}$ |
| | $\mathcal{O}(\alpha_1)$ | $\mathcal{O}(\rho_1)$ | $\mathcal{O}(\rho_2)$ | $\mathcal{O}(u_1)$ | $\mathcal{O}(u_2)$ |
| | 1.99 | 2.45 | 2.55 | 2.74 | 2.80 |
| | 2.33 | 2.82 | 2.84 | 2.62 | 2.60 |
| | 2.67 | 2.82 | 2.84 | 2.57 | 2.55 |
| | 2.81 | 2.87 | 2.90 | 2.66 | 2.64 |
| $N = 3$ | | | | | |
| $N_x = N_y$ | $L^2_\Omega(\alpha_1)$ | $L^2_\Omega(\rho_1)$ | $L^2_\Omega(\rho_2)$ | $L^2_\Omega(u_1)$ | $L^2_\Omega(u_2)$ |
| 16 | $8.284\,2 \times 10^{-4}$ | $6.252\,3 \times 10^{-3}$ | $4.210\,0 \times 10^{-3}$ | $1.350\,7 \times 10^{-2}$ | $1.153\,5 \times 10^{-2}$ |
| 32 | $3.424\,1 \times 10^{-5}$ | $2.584\,1 \times 10^{-4}$ | $2.652\,4 \times 10^{-4}$ | $1.476\,9 \times 10^{-3}$ | $1.400\,8 \times 10^{-3}$ |
| 64 | $1.447\,0 \times 10^{-6}$ | $1.302\,7 \times 10^{-5}$ | $1.008\,2 \times 10^{-5}$ | $6.961\,3 \times 10^{-5}$ | $5.541\,6 \times 10^{-5}$ |
| 96 | $2.221\,4 \times 10^{-7}$ | $2.349\,8 \times 10^{-6}$ | $1.616\,3 \times 10^{-6}$ | $1.127\,9 \times 10^{-5}$ | $8.241\,7 \times 10^{-6}$ |
| 128 | $5.948\,9 \times 10^{-8}$ | $7.618\,9 \times 10^{-7}$ | $5.479\,0 \times 10^{-7}$ | $3.259\,9 \times 10^{-6}$ | $2.298\,6 \times 10^{-6}$ |
| | $\mathcal{O}(\alpha_1)$ | $\mathcal{O}(\rho_1)$ | $\mathcal{O}(\rho_2)$ | $\mathcal{O}(u_1)$ | $\mathcal{O}(u_2)$ |
| | 4.60 | 4.60 | 3.99 | 3.19 | 3.04 |
| | 4.56 | 4.31 | 4.72 | 4.41 | 4.66 |
| | 4.62 | 4.22 | 4.51 | 4.49 | 4.70 |
| | 4.58 | 3.92 | 3.76 | 4.31 | 4.44 |
| $N = 4$ | | | | | |
| $N_x = N_y$ | $L^2_\Omega(\alpha_1)$ | $L^2_\Omega(\rho_1)$ | $L^2_\Omega(\rho_2)$ | $L^2_\Omega(u_1)$ | $L^2_\Omega(u_2)$ |
| 16 | $1.098\,4 \times 10^{-4}$ | $7.639\,7 \times 10^{-4}$ | $8.761\,6 \times 10^{-4}$ | $4.603\,7 \times 10^{-3}$ | $4.312\,4 \times 10^{-3}$ |
| 24 | $1.744\,0 \times 10^{-5}$ | $1.423\,1 \times 10^{-4}$ | $1.148\,9 \times 10^{-4}$ | $7.279\,2 \times 10^{-4}$ | $5.810\,6 \times 10^{-4}$ |
| 32 | $5.176\,8 \times 10^{-6}$ | $3.907\,9 \times 10^{-5}$ | $2.823\,9 \times 10^{-5}$ | $1.885\,0 \times 10^{-4}$ | $1.389\,5 \times 10^{-4}$ |
| 48 | $8.975\,4 \times 10^{-7}$ | $5.826\,6 \times 10^{-6}$ | $4.205\,9 \times 10^{-6}$ | $2.445\,4 \times 10^{-5}$ | $1.881\,0 \times 10^{-5}$ |
| 64 | $2.431\,7 \times 10^{-7}$ | $1.468\,2 \times 10^{-6}$ | $1.072\,0 \times 10^{-6}$ | $5.768\,7 \times 10^{-6}$ | $4.731\,6 \times 10^{-6}$ |
| | $\mathcal{O}(\alpha_1)$ | $\mathcal{O}(\rho_1)$ | $\mathcal{O}(\rho_2)$ | $\mathcal{O}(u_1)$ | $\mathcal{O}(u_2)$ |
| | 4.54 | 4.14 | 5.01 | 4.55 | 4.94 |
| | 4.22 | 4.49 | 4.88 | 4.70 | 4.97 |
| | 4.32 | 4.69 | 4.70 | 5.04 | 4.93 |
| | 4.54 | 4.79 | 4.75 | 5.02 | 4.80 |

**Table 1** (Continued)

| $N = 5$ | | | | | |
|---|---|---|---|---|---|
| $N_x = N_y$ | $L^2_\Omega(\alpha_1)$ | $L^2_\Omega(\rho_1)$ | $L^2_\Omega(\rho_2)$ | $L^2_\Omega(u_1)$ | $L^2_\Omega(u_2)$ |
| 10 | $3.104\,4 \times 10^{-4}$ | $1.818\,4 \times 10^{-3}$ | $2.253\,4 \times 10^{-3}$ | $1.073\,1 \times 10^{-2}$ | $9.972\,6 \times 10^{-3}$ |
| 20 | $9.486\,8 \times 10^{-6}$ | $6.988\,5 \times 10^{-5}$ | $3.462\,0 \times 10^{-5}$ | $2.627\,0 \times 10^{-4}$ | $1.876\,6 \times 10^{-4}$ |
| 30 | $1.306\,7 \times 10^{-6}$ | $7.625\,6 \times 10^{-6}$ | $6.993\,9 \times 10^{-6}$ | $5.217\,8 \times 10^{-5}$ | $5.066\,6 \times 10^{-5}$ |
| 40 | $2.636\,2 \times 10^{-7}$ | $1.473\,6 \times 10^{-6}$ | $1.556\,3 \times 10^{-6}$ | $1.193\,2 \times 10^{-5}$ | $1.177\,6 \times 10^{-5}$ |
| 50 | $5.659\,6 \times 10^{-8}$ | $3.657\,2 \times 10^{-7}$ | $3.890\,2 \times 10^{-7}$ | $3.078\,6 \times 10^{-6}$ | $3.006\,7 \times 10^{-6}$ |
| | $\mathcal{O}(\alpha_1)$ | $\mathcal{O}(\rho_1)$ | $\mathcal{O}(\rho_2)$ | $\mathcal{O}(u_1)$ | $\mathcal{O}(u_2)$ |
| | 5.03 | 4.70 | 6.02 | 5.35 | 5.73 |
| | 4.89 | 5.46 | 3.94 | 3.99 | 3.23 |
| | 5.56 | 5.71 | 5.22 | 5.13 | 5.07 |
| | 6.89 | 6.25 | 6.21 | 6.07 | 6.12 |

kind of nonlinear *resonance*, see [45]. The feature can best be appreciated inside the right rarefaction in the quantity $w$ in the lower right panel of Fig. 4.

### 4.3 The 2D Explosion Problems

In this section, we solve the system for multi-phase flows in two dimension in a circular computational domain with radius $R = 1$. The initial condition is given by

$$\mathbf{Q}(\mathbf{x}, t) = \begin{cases} \mathbf{Q}_{\mathrm{L}}, & \text{if } |\mathbf{x}| < 0.5, \\ \mathbf{Q}_{\mathrm{R}}, & \text{otherwise}, \end{cases} \tag{28}$$

where $\mathbf{Q}_{\mathrm{L}}$ and $\mathbf{Q}_{\mathrm{R}}$ are described in Table 5.

As a reference solution, we will solve the following equivalent (non-conservative) PDE in radial direction with geometric reaction source terms:

$$\begin{cases} \dfrac{\partial \alpha_1}{\partial t} + u^r \dfrac{\partial \alpha_1}{\partial r} = 0, & \text{(29a)} \\ \dfrac{\partial \alpha_1 \rho_1}{\partial t} + \dfrac{\partial (\alpha_1 \rho_1 u_1^r)}{\partial r} = -\dfrac{d}{r}(\alpha_1 \rho_1 u_1^r), & \text{(29b)} \\ \dfrac{\partial \alpha_2 \rho_2}{\partial t} + \dfrac{\partial (\alpha_2 \rho_2 u_2^r)}{\partial r} = -\dfrac{d}{r}(\alpha_2 \rho_2 u_2^r), & \text{(29c)} \\ \dfrac{\partial \rho u^r}{\partial t} + \dfrac{\partial (\alpha_1 \rho_1 (u_1^r)^2 + \alpha_2 \rho_2 (u_2^r)^2 + p)}{\partial r} = -\dfrac{\alpha_1 \rho_1 (u_1^r)^2}{r} - \dfrac{\alpha_2 \rho_2 (u_2^r)^2}{r}, & \text{(29d)} \\ \dfrac{\partial w^r}{\partial t} + \dfrac{\partial}{\partial r}\left( \dfrac{1}{2}(u_1^r)^2 - \dfrac{1}{2}(u_2^r)^2 + h_1 - h_2 \right) = 0, & \text{(29e)} \end{cases}$$

**Table 2** Numerical convergence rates for DG schemes of polynomial approximation $N = 2, 3, 4, 5$ with a uniform Cartesian mesh of $N_x \times N_y$ elements in the unsteady case. The $L^2$ error norms and the convergence orders of the variables $\alpha_1$, $\rho_1$, $\rho_2$, $u_1$, and $u_2$, are computed at time $t = 5$ with $\bar{u}_1 = \bar{u}_2 = 4$

| $N = 2$ | | | | | |
|---|---|---|---|---|---|
| $N_x = N_y$ | $L^2_\Omega(\alpha_1)$ | $L^2_\Omega(\rho_1)$ | $L^2_\Omega(\rho_2)$ | $L^2_\Omega(u_1)$ | $L^2_\Omega(u_2)$ |
| 16 | $2.570\,6 \times 10^{-2}$ | $1.291\,6 \times 10^{-1}$ | $1.262\,7 \times 10^{-1}$ | $2.612\,7 \times 10^{-1}$ | $2.596\,7 \times 10^{-1}$ |
| 32 | $2.832\,4 \times 10^{-3}$ | $1.429\,4 \times 10^{-2}$ | $1.402\,5 \times 10^{-2}$ | $3.346\,2 \times 10^{-2}$ | $3.277\,6 \times 10^{-2}$ |
| 64 | $3.163\,7 \times 10^{-4}$ | $1.669\,7 \times 10^{-3}$ | $1.611\,1 \times 10^{-3}$ | $3.739\,2 \times 10^{-3}$ | $3.696\,4 \times 10^{-3}$ |
| 128 | $3.564\,0 \times 10^{-5}$ | $1.979\,2 \times 10^{-4}$ | $1.877\,2 \times 10^{-4}$ | $4.182\,4 \times 10^{-4}$ | $4.145\,9 \times 10^{-4}$ |
| 256 | $4.315\,5 \times 10^{-6}$ | $2.447\,3 \times 10^{-5}$ | $2.302\,9 \times 10^{-5}$ | $5.049\,2 \times 10^{-5}$ | $5.006\,6 \times 10^{-5}$ |
| | $\mathcal{O}(\alpha_1)$ | $\mathcal{O}(\rho_1)$ | $\mathcal{O}(\rho_2)$ | $\mathcal{O}(u_1)$ | $\mathcal{O}(u_2)$ |
| | 3.18 | 3.18 | 3.17 | 2.96 | 2.99 |
| | 3.16 | 3.10 | 3.12 | 3.16 | 3.15 |
| | 3.15 | 3.08 | 3.10 | 3.16 | 3.16 |
| | 3.05 | 3.02 | 3.03 | 3.05 | 3.05 |
| $N = 3$ | | | | | |
| $N_x = N_y$ | $L^2_\Omega(\alpha_1)$ | $L^2_\Omega(\rho_1)$ | $L^2_\Omega(\rho_2)$ | $L^2_\Omega(u_1)$ | $L^2_\Omega(u_2)$ |
| 16 | $2.515\,6 \times 10^{-3}$ | $1.536\,8 \times 10^{-2}$ | $1.419\,0 \times 10^{-2}$ | $4.007\,2 \times 10^{-2}$ | $3.862\,6 \times 10^{-2}$ |
| 32 | $1.399\,6 \times 10^{-4}$ | $1.648\,9 \times 10^{-3}$ | $1.558\,0 \times 10^{-3}$ | $4.471\,5 \times 10^{-3}$ | $4.470\,6 \times 10^{-3}$ |
| 64 | $9.245\,1 \times 10^{-6}$ | $7.253\,2 \times 10^{-5}$ | $6.713\,8 \times 10^{-5}$ | $2.096\,3 \times 10^{-4}$ | $2.094\,1 \times 10^{-4}$ |
| 96 | $1.841\,9 \times 10^{-6}$ | $1.044\,6 \times 10^{-5}$ | $9.222\,0 \times 10^{-6}$ | $2.802\,8 \times 10^{-5}$ | $2.786\,0 \times 10^{-5}$ |
| 128 | $5.844\,6 \times 10^{-7}$ | $2.902\,4 \times 10^{-6}$ | $2.479\,4 \times 10^{-6}$ | $7.239\,6 \times 10^{-6}$ | $7.161\,7 \times 10^{-6}$ |
| | $\mathcal{O}(\alpha_1)$ | $\mathcal{O}(\rho_1)$ | $\mathcal{O}(\rho_2)$ | $\mathcal{O}(u_1)$ | $\mathcal{O}(u_2)$ |
| | 4.17 | 3.22 | 3.19 | 3.16 | 3.11 |
| | 3.92 | 4.51 | 4.54 | 4.41 | 4.42 |
| | 3.98 | 4.78 | 4.90 | 4.96 | 4.97 |
| | 3.99 | 4.45 | 4.57 | 4.71 | 4.72 |
| $N = 4$ | | | | | |
| $N_x = N_y$ | $L^2_\Omega(\alpha_1)$ | $L^2_\Omega(\rho_1)$ | $L^2_\Omega(\rho_2)$ | $L^2_\Omega(u_1)$ | $L^2_\Omega(u_2)$ |
| 16 | $7.243\,9 \times 10^{-4}$ | $6.496\,4 \times 10^{-3}$ | $6.220\,0 \times 10^{-3}$ | $1.705\,0 \times 10^{-2}$ | $1.695\,2 \times 10^{-2}$ |
| 24 | $7.804\,8 \times 10^{-5}$ | $9.144\,2 \times 10^{-4}$ | $8.721\,9 \times 10^{-4}$ | $2.693\,7 \times 10^{-3}$ | $2.691\,9 \times 10^{-3}$ |
| 32 | $1.475\,3 \times 10^{-5}$ | $1.663\,4 \times 10^{-4}$ | $1.542\,9 \times 10^{-4}$ | $5.433\,9 \times 10^{-4}$ | $5.425\,8 \times 10^{-4}$ |
| 48 | $1.606\,8 \times 10^{-6}$ | $1.235\,6 \times 10^{-5}$ | $9.817\,6 \times 10^{-6}$ | $4.022\,8 \times 10^{-5}$ | $4.003\,0 \times 10^{-5}$ |
| 64 | $3.806\,8 \times 10^{-7}$ | $2.486\,3 \times 10^{-6}$ | $1.737\,3 \times 10^{-6}$ | $6.272\,1 \times 10^{-6}$ | $6.203\,9 \times 10^{-6}$ |
| | $\mathcal{O}(\alpha_1)$ | $\mathcal{O}(\rho_1)$ | $\mathcal{O}(\rho_2)$ | $\mathcal{O}(u_1)$ | $\mathcal{O}(u_2)$ |
| | 5.49 | 4.84 | 4.85 | 4.55 | 4.54 |
| | 5.79 | 5.92 | 6.02 | 5.56 | 5.57 |
| | 5.47 | 6.41 | 6.79 | 6.42 | 6.43 |
| | 5.01 | 5.57 | 6.02 | 6.46 | 6.48 |

**Table 2** (Continued)

| $N = 5$ | | | | | |
|---|---|---|---|---|---|
| $N_x = N_y$ | $L^2_\Omega(\alpha_1)$ | $L^2_\Omega(\rho_1)$ | $L^2_\Omega(\rho_2)$ | $L^2_\Omega(u_1)$ | $L^2_\Omega(u_2)$ |
| 10 | $2.053\,2 \times 10^{-3}$ | $1.479\,8 \times 10^{-2}$ | $1.380\,7 \times 10^{-2}$ | $3.583\,1 \times 10^{-2}$ | $3.509\,0 \times 10^{-2}$ |
| 20 | $2.970\,1 \times 10^{-5}$ | $3.416\,9 \times 10^{-4}$ | $3.193\,8 \times 10^{-4}$ | $1.160\,6 \times 10^{-3}$ | $1.157\,2 \times 10^{-3}$ |
| 30 | $2.284\,5 \times 10^{-6}$ | $1.893\,5 \times 10^{-5}$ | $1.674\,3 \times 10^{-5}$ | $8.309\,4 \times 10^{-5}$ | $8.291\,5 \times 10^{-5}$ |
| 40 | $3.849\,3 \times 10^{-7}$ | $3.193\,2 \times 10^{-6}$ | $2.727\,4 \times 10^{-6}$ | $1.177\,0 \times 10^{-5}$ | $1.175\,4 \times 10^{-5}$ |
| 50 | $9.482\,8 \times 10^{-8}$ | $9.692\,8 \times 10^{-7}$ | $8.349\,6 \times 10^{-7}$ | $3.172\,6 \times 10^{-6}$ | $3.167\,1 \times 10^{-6}$ |
| | $\mathcal{O}(\alpha_1)$ | $\mathcal{O}(\rho_1)$ | $\mathcal{O}(\rho_2)$ | $\mathcal{O}(u_1)$ | $\mathcal{O}(u_2)$ |
| | 6.11 | 5.44 | 5.43 | 4.95 | 4.92 |
| | 6.33 | 7.13 | 7.27 | 6.50 | 6.50 |
| | 6.19 | 6.19 | 6.31 | 6.79 | 6.79 |
| | 6.28 | 5.34 | 5.30 | 5.88 | 5.88 |

**Table 3** Numerical convergence rates for DG schemes with $N = 3$ using a uniform Cartesian mesh of $N_x \times N_y$ elements in the unsteady case using the original system (4), the augmented system with the GLM approach (12), and the system with the Godunov-Powell terms (14). The $L^2$ error norms and the convergence orders of the variables $\alpha_1$, $\rho_1$, $\rho_2$, $u_1$, and $u_2$, are computed at time $t = 5$ with $\bar{u}_1 = \bar{u}_2 = 4$

| $N = 3$, original system | | | | | |
|---|---|---|---|---|---|
| $N_x = N_y$ | $L^2_\Omega(\alpha_1)$ | $L^2_\Omega(\rho_1)$ | $L^2_\Omega(\rho_2)$ | $L^2_\Omega(u_1)$ | $L^2_\Omega(u_2)$ |
| 16 | $2.515\,6 \times 10^{-3}$ | $1.536\,8 \times 10^{-2}$ | $1.419\,0 \times 10^{-2}$ | $4.007\,2 \times 10^{-2}$ | $3.862\,6 \times 10^{-2}$ |
| 32 | $1.399\,6 \times 10^{-4}$ | $1.648\,9 \times 10^{-3}$ | $1.558\,0 \times 10^{-3}$ | $4.471\,5 \times 10^{-3}$ | $4.470\,6 \times 10^{-3}$ |
| 64 | $9.245\,1 \times 10^{-6}$ | $7.253\,2 \times 10^{-5}$ | $6.713\,8 \times 10^{-5}$ | $2.096\,3 \times 10^{-4}$ | $2.094\,1 \times 10^{-4}$ |
| 128 | $5.844\,6 \times 10^{-7}$ | $2.902\,4 \times 10^{-6}$ | $2.479\,4 \times 10^{-6}$ | $7.239\,6 \times 10^{-6}$ | $7.161\,7 \times 10^{-6}$ |
| 256 | $3.691\,6 \times 10^{-8}$ | $1.595\,8 \times 10^{-7}$ | $1.329\,7 \times 10^{-7}$ | $3.601\,5 \times 10^{-7}$ | $3.544\,9 \times 10^{-7}$ |
| | $\mathcal{O}(\alpha_1)$ | $\mathcal{O}(\rho_1)$ | $\mathcal{O}(\rho_2)$ | $\mathcal{O}(u_1)$ | $\mathcal{O}(u_2)$ |
| | 4.17 | 3.22 | 3.19 | 3.16 | 3.11 |
| | 3.92 | 4.51 | 4.54 | 4.41 | 4.42 |
| | 3.98 | 4.64 | 4.76 | 4.86 | 4.87 |
| | 3.98 | 4.18 | 4.22 | 4.33 | 4.34 |
| $N = 3$, GLM approach | | | | | |
| $N_x = N_y$ | $L^2_\Omega(\alpha_1)$ | $L^2_\Omega(\rho_1)$ | $L^2_\Omega(\rho_2)$ | $L^2_\Omega(u_1)$ | $L^2_\Omega(u_2)$ |
| 16 | $2.515\,5 \times 10^{-3}$ | $1.532\,9 \times 10^{-2}$ | $1.422\,5 \times 10^{-2}$ | $3.983\,5 \times 10^{-2}$ | $3.883\,8 \times 10^{-2}$ |
| 32 | $1.399\,6 \times 10^{-4}$ | $1.649\,0 \times 10^{-3}$ | $1.557\,9 \times 10^{-3}$ | $4.473\,0 \times 10^{-3}$ | $4.469\,0 \times 10^{-3}$ |
| 64 | $9.237\,5 \times 10^{-6}$ | $7.250\,7 \times 10^{-5}$ | $6.713\,0 \times 10^{-5}$ | $2.095\,6 \times 10^{-4}$ | $2.094\,0 \times 10^{-4}$ |
| 128 | $5.858\,5 \times 10^{-7}$ | $2.884\,5 \times 10^{-6}$ | $2.476\,2 \times 10^{-6}$ | $7.126\,0 \times 10^{-6}$ | $7.067\,7 \times 10^{-6}$ |
| 256 | $3.691\,6 \times 10^{-8}$ | $1.594\,2 \times 10^{-7}$ | $1.331\,0 \times 10^{-7}$ | $3.599\,8 \times 10^{-7}$ | $3.546\,1 \times 10^{-7}$ |

**Table 3** (Continued)

| | $\mathcal{O}(\alpha_1)$ | $\mathcal{O}(\rho_1)$ | $\mathcal{O}(\rho_2)$ | $\mathcal{O}(u_1)$ | $\mathcal{O}(u_2)$ |
|---|---|---|---|---|---|
| | 4.17 | 3.22 | 3.19 | 3.15 | 3.12 |
| | 3.92 | 4.51 | 4.54 | 4.42 | 4.42 |
| | 3.98 | 4.65 | 4.76 | 4.88 | 4.89 |
| | 3.99 | 4.18 | 4.22 | 4.31 | 4.32 |
| $N = 3$, Godunov-Powell terms | | | | | |
| $N_x = N_y$ | $L^2_\Omega(\alpha_1)$ | $L^2_\Omega(\rho_1)$ | $L^2_\Omega(\rho_2)$ | $L^2_\Omega(u_1)$ | $L^2_\Omega(u_2)$ |
| 16 | $2.515\,6 \times 10^{-3}$ | $1.536\,8 \times 10^{-2}$ | $1.419\,0 \times 10^{-2}$ | $4.007\,2 \times 10^{-2}$ | $3.862\,5 \times 10^{-2}$ |
| 32 | $1.399\,6 \times 10^{-4}$ | $1.648\,9 \times 10^{-3}$ | $1.558\,0 \times 10^{-3}$ | $4.471\,5 \times 10^{-3}$ | $4.470\,6 \times 10^{-3}$ |
| 64 | $9.237\,5 \times 10^{-6}$ | $7.251\,5 \times 10^{-5}$ | $6.712\,1 \times 10^{-5}$ | $2.095\,9 \times 10^{-4}$ | $2.093\,7 \times 10^{-4}$ |
| 128 | $5.858\,5 \times 10^{-7}$ | $2.886\,5 \times 10^{-6}$ | $2.474\,7 \times 10^{-6}$ | $7.133\,0 \times 10^{-6}$ | $7.060\,8 \times 10^{-6}$ |
| 256 | $3.691\,6 \times 10^{-8}$ | $1.595\,8 \times 10^{-7}$ | $1.329\,7 \times 10^{-7}$ | $3.601\,5 \times 10^{-7}$ | $3.544\,9 \times 10^{-7}$ |
| | $\mathcal{O}(\alpha_1)$ | $\mathcal{O}(\rho_1)$ | $\mathcal{O}(\rho_2)$ | $\mathcal{O}(u_1)$ | $\mathcal{O}(u_2)$ |
| | 4.17 | 3.22 | 3.19 | 3.16 | 3.11 |
| | 3.92 | 4.51 | 4.54 | 4.42 | 4.42 |
| | 3.98 | 4.65 | 4.76 | 4.88 | 4.89 |
| | 3.99 | 4.18 | 4.22 | 4.31 | 4.32 |

**Table 4** Left and right states of the Riemann problem 1

| | $\alpha$ | $\rho_1$ | $\rho_2$ | $u_1$ | $u_2$ |
|---|---|---|---|---|---|
| $Q_L$ | 0.7 | 1.244 9 | 1.296 9 | −1.263 8 | −0.389 47 |
| $Q_R$ | 0.3 | 0.603 12 | 0.734 36 | 0.430 59 | −0.405 07 |

where the parameter $d$ is the number of spatial dimensions minus one. The 2D computations have been performed using a fourth-order ($N = 3$) ADER-DG scheme with *a posteriori* subcell limiter. The computational domain is $\Omega = [-1, 1] \times [-1, 1]$ and has been discretized using a Cartesian mesh with $512 \times 512$ elements. Following (28), the left state of the Riemann problem has been taken as the inner state and the right state of the same Riemann problem as the outer state. The reference solution has been computed by solving (29) with 128 000 cells using a second-order TVD finite-volume method with the Rusanov flux. The simulation is performed up to $t = 0.1$ with two ideal gases, so, for the two phases, the EOS is given by (6) with $s_i = 0$, $\gamma_1 = 1.4$, and $\gamma_2 = 2$, respectively.

Figures 5 and 6 show the numerical results of two circular explosion problems with the initial conditions of Table 5 and a final time of $t = 0.1$ for the first one and $t = 0.2$ for the second one. The numerical solution obtained with the ADER-DG method is then compared with the radial reference solution, showing excellent agreement. Moreover, Fig. 7 shows the limiter map of the second explosion problem. The values highlighted in blue are those DG elements where the limiter is not activated, and the red ones are the troubled zones where the *a posteriori* subcell finite-volume limiter is activated.

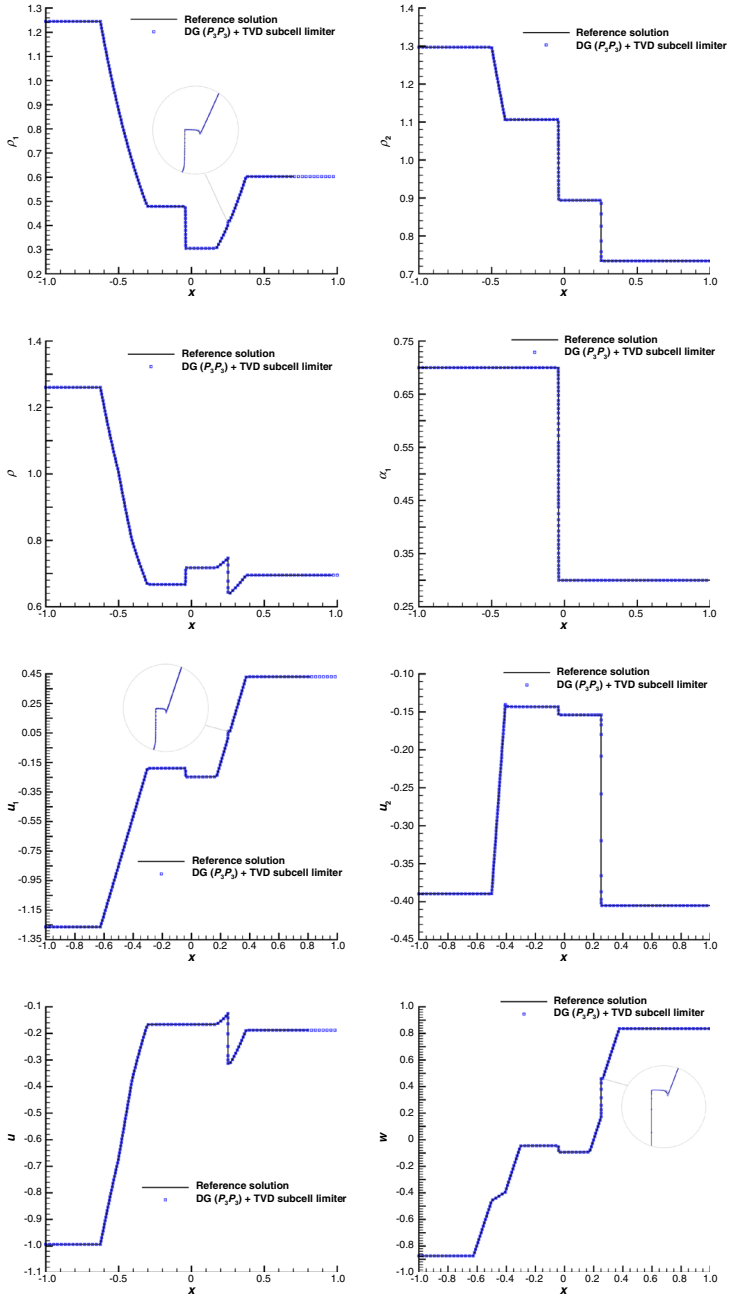


**Fig. 4** The 1D Riemann problem solved with a fourth-order ADER-DG scheme with the TVD subcell limiter on a Cartesian mesh with 8 192 cells at time $t = 0.25$. Top row: densities of each phase, $\rho_1$ and $\rho_2$. Second row: the mixture density $\rho$ and $\alpha$. Third row: the velocities $u_1$ and $u_2$. Bottom row: the mixture velocity $u$ (left) and relative velocity $w = u_1 - u_2$ (right)

**Table 5** Left and right states of the circular explosion problems

| CE1 | | | | | | | | | |
|---|---|---|---|---|---|---|---|---|---|
| | $\alpha$ | $\rho_1$ | $\rho_2$ | $u_1^1$ | $u_1^2$ | $u_1^3$ | $u_2^1$ | $u_2^2$ | $u_2^2$ |
| $\mathbf{Q}_\mathrm{L}$ | 0.4 | 2 | 1.5 | 0 | 0 | 0 | 0 | 0 | 0 |
| $\mathbf{Q}_\mathrm{R}$ | 0.8 | 1 | 0.5 | 0 | 0 | 0 | 0 | 0 | 0 |
| CE2 | | | | | | | | | |
| | $\alpha$ | $\rho_1$ | $\rho_2$ | $u_1^1$ | $u_1^2$ | $u_1^3$ | $u_2^1$ | $u_2^2$ | $u_2^2$ |
| $\mathbf{Q}_\mathrm{L}$ | 0.7 | 1 | 2 | 0 | 0 | 0 | 0 | 0 | 0 |
| $\mathbf{Q}_\mathrm{R}$ | 0.3 | 2 | 1 | 0 | 0 | 0 | 0 | 0 | 0 |

### 4.4 Dambreak Problem

Finally, a 2D dambreak problem is solved using the barotropic two-phase model studied in this paper. In this case, the source term included in the momentum Eq. (4d) is non-zero, as a non-zero gravity source is considered, and hence, $\boldsymbol{g} = (0, -g, 0)$ with $g = 9.81$. The computational domain is $\Omega = [0, 4] \times [0, 2]$, where the water domain is $\Omega_2 = [0, 2] \times [0, 1]$ and the air domain is given by $\Omega_1 = \Omega \backslash \Omega_2$.

The domain $\Omega$ has been discretized with a uniform Cartesian mesh with $256 \times 128$ cells, using an ADER-DG scheme with $N = 3$ and *a posteriori* subcell finite-volume limiter. The simulation has been performed until a final time of $t = 0.4$, and a slip wall boundary condition is imposed on all boundaries. Following Sect. 2.1, an ideal gas is considered in $\Omega_1$, i.e., the EOS is given by (5) with parameters $c_{01} = 1$, $\gamma_1 = 1.4$, $\rho_{01} = 1$, $\alpha = \varepsilon$. The initial pressure profile is assumed hydrostatic, $p = \rho_{01} g(y - 2)$. The EOS for the liquid is a stiffened gas EOS given by (7), where $c_{02} = 20$, $\gamma_2 = 2$, $\rho_{02} = 1\,000$, $\alpha = 1 - \varepsilon$, and again a hydrostatic pressure profile $p = \rho_{02} g(y - 1)$ is imposed initially. The simulation was performed with $\varepsilon = 0$, i.e., initially, the phase volume fractions are really set to zero and unity, respectively. To obtain the value of the primitive variable $\rho_k$, it is necessary to divide by $\alpha_k$, and in this simulation, there exist areas with $\alpha_k = 0$, and it is necessary to apply a *filter* that avoids division by zero. In this paper, the density variables are filtered as follows:

$$\rho_k = \frac{\rho_k {\alpha_k}^2 + \rho_{0k} \epsilon}{\alpha_k^2 + \epsilon},$$

see also [68], and the filter parameter is set $\epsilon = 10^{-12}$. The numerical results have been compared with the solution of the reduced barotropic BN model given in [25]. Figure 8 shows the values obtained at time $t = 0.4$ calculated with the reduced BN model in the upper plot, the solution calculated with the method proposed in this paper in the center, and a direct comparison of both models with the solution for the augmented model with the GLM approach and for the system with the Godunov-Powell terms, in the bottom plot, showing an excellent agreement among all the models. Similar results have also been recently obtained with a novel Arbitrary-Lagrangian-Eulerian hybrid finite-volume/finite-element method applied to the incompressible Navier-Stokes equations on moving unstructured meshes, see [12].

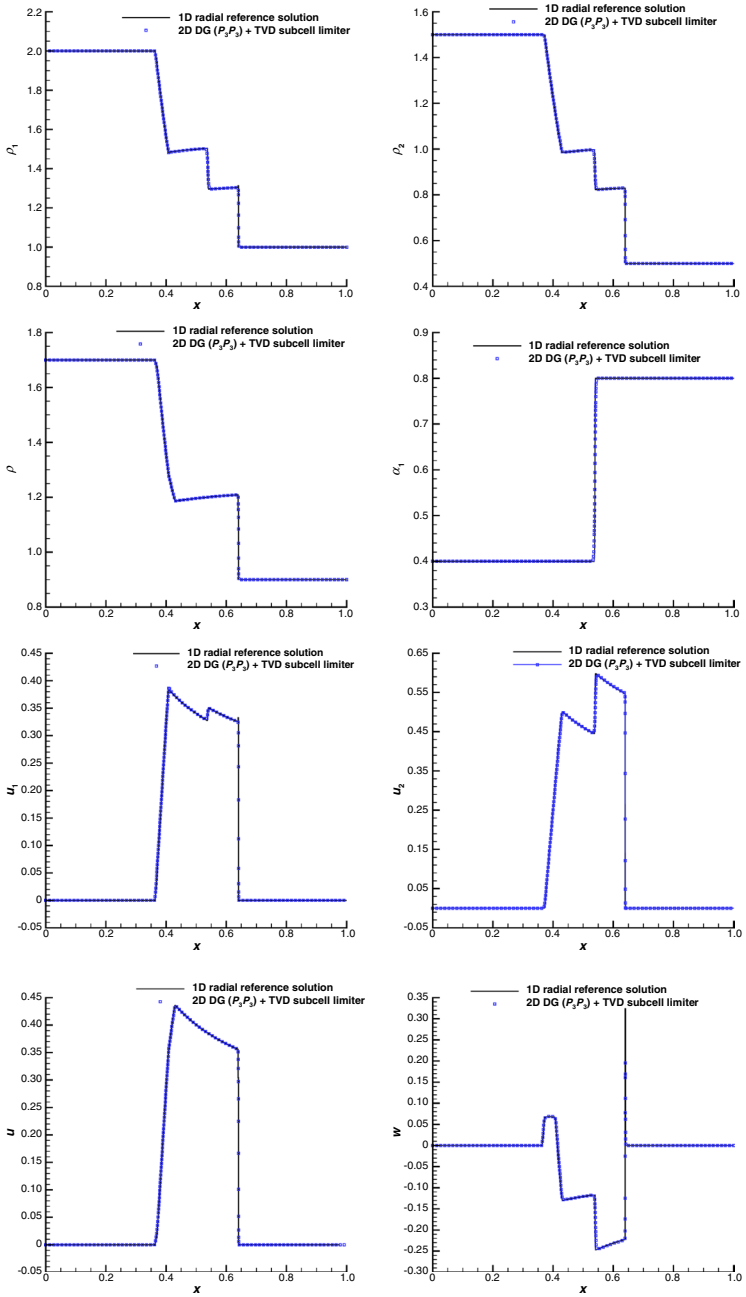


**Fig. 5** The 2D circular explosion problem for the initial condition CE1 in Table 5 solved on a Cartesian mesh at time $t = 0.1$, in comparison with the radial reference solution. Top row: densities of each phase, $\rho_1$ and $\rho_2$. Second row: the mixture density $\rho$ and $\alpha$. Third row: the velocities $u_1$ and $u_2$. Bottom row: the mixture velocity $u$ (left) and relative velocity $w = u_1 - u_2$ (right)

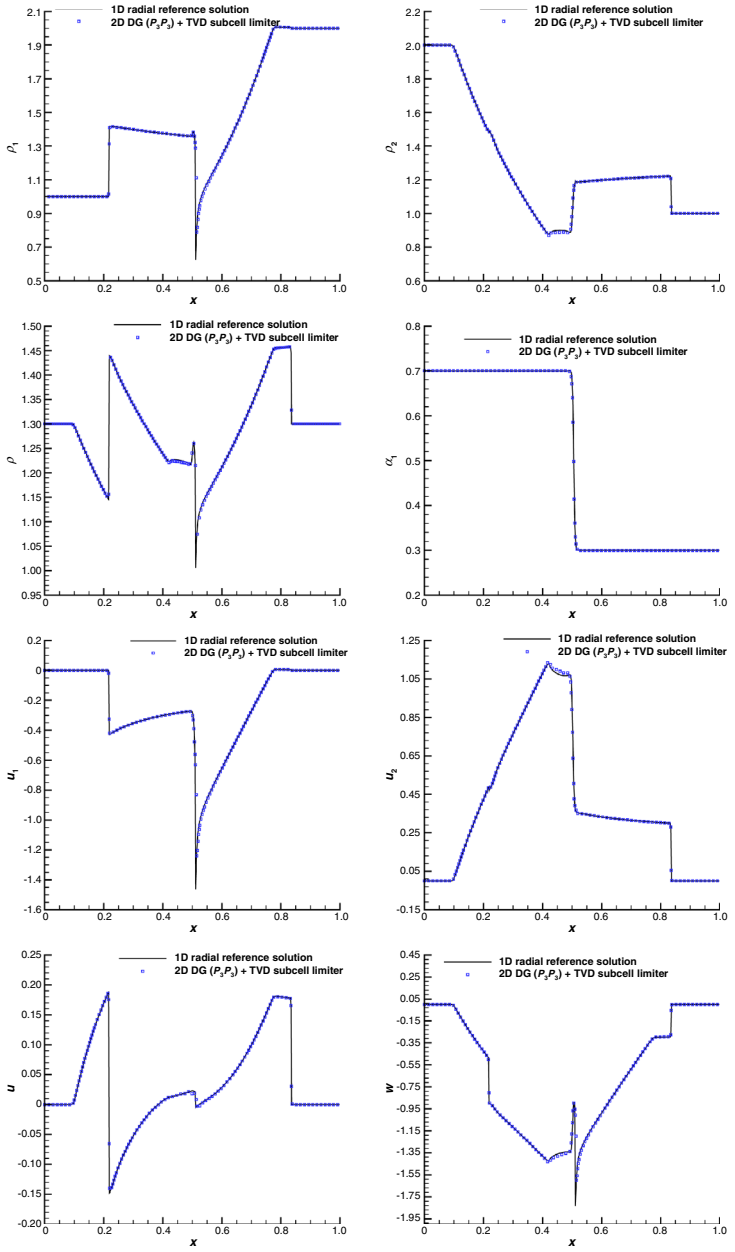


**Fig. 6** The 2D circular explosion problem for the initial condition CE2 in Table 5 solved on a Cartesian mesh at time $t = 0.2$, compared with the radial reference solution. Top row: densities of each phase, $\rho_1$ and $\rho_2$. Second row: the mixture density $\rho$ and $\alpha$. Third row: the velocities $u_1$ and $u_2$. Bottom row: the mixture velocity $u$ (left) and relative velocity $w = u_1 - u_2$ (right)

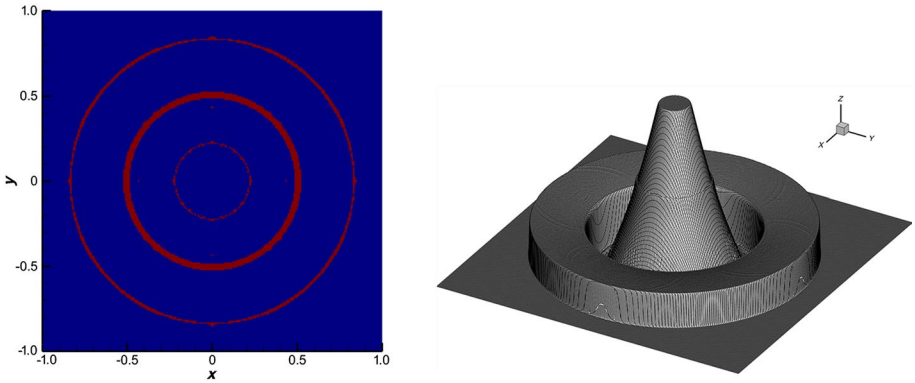


**Fig. 7** Left: the limiter map of the explosion problem in two dimensions. The values in red mean that the limiter is activated. Right: the 3D plot with the variable $\rho_2$ in the $z$-axis

## 5 Conclusion

In this paper, the barotropic version of the conservative SHTC model for compressible two-fluid flows of Romenski et al. has been solved for the first time using high-order ADER-DG schemes in combination with *a posteriori* subcell finite-volume limiter. Since the model is only weakly hyperbolic in the general multidimensional case, two different methodologies have been presented to restore the strong hyperbolicity: (i) a GLM curl-cleaning approach; (ii) the addition of the Godunov-Powell terms to symmetrize the system. We obtain a full set of linearly independent eigenvectors with both methodologies, proving that strong hyperbolicity can indeed be restored.

A high-order ADER-DG finite-element scheme with *a posteriori* subcell finite-volume limiter has been used to deal with discontinuities and steep gradients in the solutions. To validate the model and the proposed method, a numerical convergence analysis has been carried out. For this purpose, we have constructed a new exact analytical and stationary equilibrium solution of the PDE system in cylindrical coordinates, and the high order of the method has been confirmed. A detailed comparison among the results obtained for the original system, for the augmented GLM curl-cleaning system, and for the Godunov-Powell-type system has been carried out, showing very similar results. Then, several Riemann problems in one and two dimensions have been simulated to show the behavior of the proposed methodology in the presence of shocks. First, a 1D Riemann problem where a shock in one phase appears inside the rarefaction of the other phase has been simulated. The results have been compared with those presented in [69], showing an excellent agreement. Then, two 2D explosion problems were solved. Thanks to the radial symmetry of the problem, the obtained results have been compared with an equivalent 1D reference solution, showing the accuracy of the proposed methodology even in the presence of sharp gradients in the solution. Finally, a dambreak test case has been considered, where the initial values of the volume fractions are set to $\alpha_1 = 0$ and $\alpha_2 = 1$. The numerical results obtained with the original system, with the augmented GLM system, and with the Godunov-Powell-type system are compared with those obtained for a reduced barotropic BN-type model, showing an excellent agreement between all the models. We can conclude that the results obtained with the original system, as well as those obtained with the GLM curl-cleaning approach and with the symmetrization of the system by adding

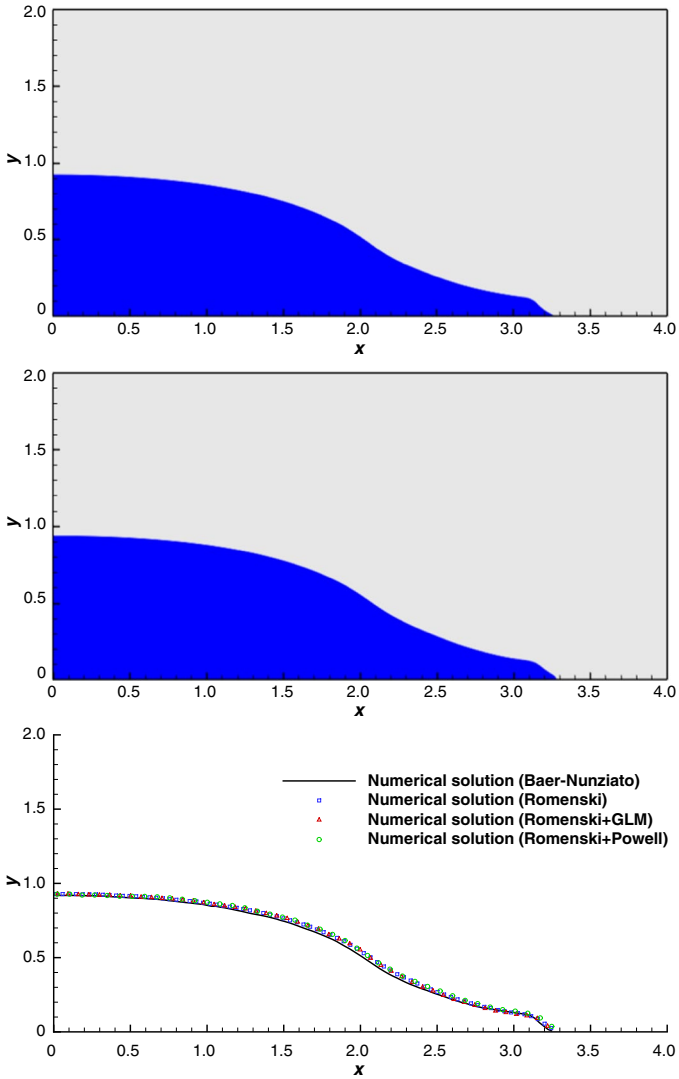


**Fig. 8** The dambreak problem at time $t = 0.4$. Top: the reference solution, computed with a third-order ADER-WENO finite-volume scheme on a very fine uniform Cartesian grid, solving the inviscid and barotropic reduced BN model presented in [25]. Center: the numerical solution, computed using an ADER-DG scheme with *a posteriori* subcell limiter, to solve the barotropic SHTC model proposed in this work. Bottom: the comparison of the free-surface profile obtained for the reduced BN model, the original model solved in this paper, the augmented model with the GLM approach, and the model including the Godunov-Powell terms

the Godunov-Powell terms, are very similar at least for all the proposed tests and do not present evidence on which method is better for this type of model.

As future work, we plan to extend our methodology to compressible multi-phase flows with more than two phases and, in addition, to include also solids governed by the equations of nonlinear hyperelasticity, see, e.g., [32, 60, 61]. Furthermore, we will also apply exactly curl-free

methods to the two-phase model discussed in this paper, such as the curl-free schemes recently forwarded in [6, 9, 15, 21].

**Acknowledgements** This research was funded by the Italian Ministry of Education, University and Research (MIUR) in the frame of the Departments of Excellence Initiative 2018–2027 attributed to DICAM of the University of Trento (grant L. 232/2016), by the PRIN 2022 project *High-order structure-preserving semi-implicit schemes for hyperbolic equations* and by the European Union-Next GenerationEU (PNRR, Spoke 7 CN HPC). Views and opinions expressed are, however, those of the author(s) only and do not necessarily reflect those of the European Union or the European Research Council. Neither the European Union nor the granting authority can be held responsible for them. L.R. acknowledges funding from the Spanish Ministry of Universities and the European Union-Next GenerationEU under the project RSU.UDC.MS15. MD and LR are members of the GNCS group of INdAM. The authors would like to acknowledge support from the CESGA, Spain, for the access to the FT3 supercomputer and to the CINECA award under the ISCRA initiative, for the availability of high-performance computing resources and support (Projects No. IsCa3_NuMFluS and NeMesiS). L. R. gratefully acknowledges Dr. Firas Dhaouadi and Dr. Ilya Peshkov for the interesting discussions and support that have allowed the successful development of this work.

**Funding** Open access funding provided by Università degli Studi di Trento within the CRUI-CARE Agreement.

**Data Availability** The data can be obtained from the authors on reasonable request.

## Compliance with Ethical Standards

**Conflict of Interest** The authors declare that they have no conflict of interest.

**Ethical Standards** The authors declare that they have complied with the commonly accepted ethical standards on Good Scientific Practice to the best of their knowledge. All funding sources have been declared in the previous Acknowledgments section.

**Ethical Approval** This work concerns basic research in applied mathematics and does not involve any experiments on humans or animals, and hence, no ethical approval was needed for this research.

**Open Access** This article is licensed under a Creative Commons Attribution 4.0 International License, which permits use, sharing, adaptation, distribution and reproduction in any medium or format, as long as you give appropriate credit to the original author(s) and the source, provide a link to the Creative Commons licence, and indicate if changes were made. The images or other third party material in this article are included in the article's Creative Commons licence, unless indicated otherwise in a credit line to the material. If material is not included in the article's Creative Commons licence and your intended use is not permitted by statutory regulation or exceeds the permitted use, you will need to obtain permission directly from the copyright holder. To view a copy of this licence, visit http://creativecommons.org/licenses/by/4.0/.

## References

1. Abgrall, R., Saurel, R.: Discrete equations for physical and numerical compressible multiphase mixtures. J. Comput. Phys. **186**(2), 361–396 (2003)
2. Anderson, D.M., McFadden, G.B., Wheeler, A.A.: Diffuse-interface methods in fluid mechanics. Annu. Rev. Fluid Mech. **30**(1), 139–165 (1998)
3. Andrianov, N., Warnecke, G.: The Riemann problem for the Baer-Nunziato two-phase flow model. J. Comput. Phys. **195**(2), 434–464 (2004)
4. Baer, M.R., Nunziato, J.W.: A two-phase mixture theory for the deflagration-to-detonation transition (DDT) in reactive granular materials. Int. J. Multiph. Flow **12**(6), 861–889 (1986)
5. Balsara, D.S.: Second-order accurate schemes for magnetohydrodynamics with divergence-free reconstruction. Astrophys. J. Suppl. Ser. **151**(1), 149 (2004)
6. Balsara, D.S., Käppeli, R., Boscheri, W., Dumbser, M.: Curl constraint-preserving reconstruction and the guidance it gives for mimetic scheme design. Commun. Appl. Math. Comput. Sci. **5**(1), 235–294 (2023)

7. Barton, P.T.: An interface-capturing Godunov method for the simulation of compressible solid-fluid problems. J. Comput. Phys. **390**, 25–50 (2019)
8. Bdzil, J.B., Menikoff, R., Son, S.F., Kapila, A.K., Stewart, D.S.: Two-phase modeling of deflagration-to-detonation transition in granular materials: a critical examination of modeling issues. Phys. Fluids **11**(2), 378–402 (1999)
9. Boscheri, W., Dumbser, M., Ioriatti, M., Peshkov, I., Romenski, E.I.: A structure-preserving staggered semi-implicit finite volume scheme for continuum mechanics. J. Comput. Phys. **424**, 2 (2021)
10. Busto, S., Chiocchetti, S., Dumbser, M., Gaburro, E., Peshkov, I.: High order ADER schemes for continuum mechanics. Front. Phys. **8**, 32 (2020)
11. Busto, S., Dumbser, M., Escalante, C., Gavrilyuk, S., Favrie, N.: On high order ADER discontinuous Galerkin schemes for first order hyperbolic reformulations of nonlinear dispersive systems. J. Sci. Comput. **87**, 25 (2021)
12. Busto, S., Dumbser, M., Río-Martín, L.: An Arbitrary-Lagrangian-Eulerian hybrid finite volume/finite element method on moving unstructured meshes for the Navier-Stokes equations. Appl. Math. Comput. **437**, 25 (2023)
13. Castro, M.J., Gallardo, J.M., Parés, C.: High-order finite volume schemes based on reconstruction of states for solving hyperbolic systems with nonconservative products. Applications to shallow-water systems. Math. Comput. **75**, 1103–1134 (2006)
14. Casulli, V.: A semi-implicit numerical method for the free-surface Navier-Stokes equations. Int. J. Numer. Meth. Fluids **74**, 605–622 (2014)
15. Chiocchetti, S., Dumbser, M.: An exactly curl-free staggered semi-implicit finite volume scheme for a first order hyperbolic model of viscous two-phase flows with surface tension. J. Sci. Comput. **94**, 2 (2023)
16. Chiocchetti, S., Peshkov, I., Gavrilyuk, S., Dumbser, M.: High order ADER schemes and GLM curl cleaning for a first order hyperbolic formulation of compressible flow with surface tension. J. Comput. Phys. **426**, 109898 (2021)
17. Clain, S., Diot, S., Loubère, R.: A high-order finite volume method for systems of conservation laws—multi-dimensional optimal order detection (MOOD). J. Comput. Phys. **230**(10), 4028–4050 (2011)
18. De Lorenzo, M., Pelanti, M., Lafon, P.: HLLC-type and path-conservative schemes for a single-velocity six-equation two-phase flow model: a comparative study. Appl. Math. Comput. **333**, 95–117 (2018)
19. Dedner, A., Kemm, F., Kröner, D., Munz, C.D., Schnitzer, T., Wesenberg, M.: Hyperbolic divergence cleaning for the MHD equations. J. Comput. Phys. **175**(2), 645–673 (2002)
20. Dhaouadi, F., Dumbser, M.: A first order hyperbolic reformulation of the Navier-Stokes-Korteweg system based on the GPR model and an augmented Lagrangian approach. J. Comput. Phys. **470**, 2 (2022)
21. Dhaouadi, F., Dumbser, M.: A structure-preserving finite volume scheme for a hyperbolic reformulation of the Navier-Stokes-Korteweg equations. Mathematics **11**, 2 (2023)
22. Diot, S., Clain, S., Loubère, R.: Improved detection criteria for the multi-dimensional optimal order detection (MOOD) on unstructured meshes with very high-order polynomials. Comput. Fluids **64**, 43–63 (2012)
23. Diot, S., Loubère, R., Clain, S.: The MOOD method in the three-dimensional case: very high-order finite volume method for hyperbolic systems. Int. J. Numer. Methods Fluids **73**, 362–392 (2013)
24. Dumbser, M.: Arbitrary high order $P_N P_M$ schemes on unstructured meshes for the compressible Navier-Stokes equations. Comput. Fluids **39**(1), 60–76 (2010)
25. Dumbser, M.: A simple two-phase method for the simulation of complex free surface flows. Comput. Methods Appl. Mech. Eng. **200**(9), 1204–1219 (2011)
26. Dumbser, M., Balsara, D.S.: High-order unstructured one-step $P_N P_M$ schemes for the viscous and resistive MHD equations. Comput. Model. Eng. Sci. (CMES) **54**(3), 301–333 (2009)
27. Dumbser, M., Balsara, D.S., Toro, E.F., Munz, C.D.: A unified framework for the construction of one-step finite volume and discontinuous Galerkin schemes on unstructured meshes. J. Comput. Phys. **227**(18), 8209–8253 (2008)
28. Dumbser, M., Enaux, C., Toro, E.F.: Finite volume schemes of very high order of accuracy for stiff hyperbolic balance laws. J. Comput. Phys. **227**(8), 3971–4001 (2008)
29. Dumbser, M., Fambri, F., Gaburro, E., Reinarz, A.: On GLM curl cleaning for a first order reduction of the CCZ4 formulation of the Einstein field equations. J. Comput. Phys. **404**, 109088 (2020)
30. Dumbser, M., Hidalgo, A., Castro, M., Parés, C., Toro, E.F.: FORCE schemes on unstructured meshes II: non-conservative hyperbolic systems. Comput. Methods Appl. Mech. Eng. **199**, 625–647 (2010)
31. Dumbser, M., Loubère, R.: A simple robust and accurate a posteriori sub-cell finite volume limiter for the discontinuous Galerkin method on unstructured meshes. J. Comput. Phys. **319**, 163–199 (2016)

32. Dumbser, M., Peshkov, I., Romenski, E.I., Zanotti, O.: High order ADER schemes for a unified first order hyperbolic formulation of continuum mechanics: viscous heat-conducting fluids and elastic solids. J. Comput. Phys. **314**, 824–862 (2016)
33. Dumbser, M., Zanotti, O.: Very high order $P_N P_M$ schemes on unstructured meshes for the resistive relativistic MHD equations. J. Comput. Phys. **228**(18), 6991–7006 (2009)
34. Dumbser, M., Zanotti, O., Loubère, R., Diot, S.: A posteriori subcell limiting of the discontinuous Galerkin finite element method for hyperbolic conservation laws. J. Comput. Phys. **278**, 47–75 (2014)
35. Favrie, N., Gavrilyuk, S.L.: Diffuse interface model for compressible fluid-compressible elastic-plastic solid interaction. J. Comput. Phys. **231**(7), 2695–2723 (2012)
36. Favrie, N., Gavrilyuk, S.L., Saurel, R.: Solid-fluid diffuse interface model in cases of extreme deformations. J. Comput. Phys. **228**(16), 6037–6077 (2009)
37. Ferrari, D., Dumbser, M.: A mass and momentum-conservative semi-implicit finite volume scheme for complex nonhydrostatic free surface flows. Int. J. Numer. Meth. Fluids **93**, 2946–2967 (2021)
38. Ferrari, D., Dumbser, M.: A semi-implicit finite volume scheme for incompressible two-phase flows. Communications on Applied Mathematics and Computation (2023). Submitted
39. Gaburro, E., Castro, M.J., Dumbser, M.: A well balanced diffuse interface method for complex non-hydrostatic free surface flows. Comput. Fluids **175**, 180–198 (2018)
40. Gassner, G., Lörcher, F., Munz, C.D.: A contribution to the construction of diffusion fluxes for finite volume and discontinuous Galerkin schemes. J. Comput. Phys. **224**(8), 1049–1063 (2007)
41. Gavrilyuk, S., Saurel, R.: Mathematical and numerical modeling of two-phase compressible flows with micro-inertia. J. Comput. Phys. **175**(1), 326–360 (2002)
42. Godunov, S.K.: An interesting class of quasi-linear systems. Dokl. Akad. Nauk SSSR **139**(3), 521–523 (1961)
43. Godunov, S.K.: Symmetric form of the magnetohydrodynamic equation. Numer. Methods Mech. Contin. Medium **3**(1), 26–34 (1972)
44. Godunov, S.K., Romenski, E.I.: Elements of Continuum Mechanics and Conservation Laws. Kluwer Academic/Plenum Publishers, Berlin (2003)
45. Isaacson, E., Temple, B.: Nonlinear resonance in systems of conservation laws. SIAM J. Appl. Math. **52**, 1260–1278 (1992)
46. Kapila, A.K., Menikoff, R., Bdzil, J.B., Son, S.F., Stewart, D.S.: Two-phase modeling of deflagration-to-detonation transition in granular materials: reduced equations. Phys. Fluids **13**(10), 3002–3024 (2001)
47. Kemm, F., Gaburro, E., Thein, F., Dumbser, M.: A simple diffuse interface approach for compressible flows around moving solids of arbitrary shape based on a reduced Baer-Nunziato model. Comput. Fluids **204**, 104536 (2020)
48. Lukáčová-Medvid'ová, M., Puppo, G., Thomann, A.: An all Mach number finite volume method for isentropic two-phase flow. J. Numer. Math. **31**(3), 175–204 (2023)
49. Munz, C.D., Omnes, P., Schneider, R., Sonnendrücker, E., Voss, U.: Divergence correction techniques for Maxwell solvers based on a hyperbolic model. J. Comput. Phys. **161**(2), 484–511 (2000)
50. Ndanou, S., Favrie, N., Gavrilyuk, S.L.: Multi-solid and multi-fluid diffuse interface model: applications to dynamic fracture and fragmentation. J. Comput. Phys. **295**, 523–555 (2015)
51. Parés, C.: Numerical methods for nonconservative hyperbolic systems: a theoretical framework. SIAM J. Numer. Anal. **44**, 300–321 (2006)
52. Powell, K.G.: An approximate Riemann solver for magnetohydrodynamics (that works in more than one dimension). Tech. Rep. ICASE-Report 94-24 (NASA CR-194902), NASA Langley Research Center, Hampton, VA (1994)
53. Powell, K.G.: An Approximate Riemann Solver for Magnetohydrodynamics, pp. 570–583. Springer, Berlin (1997)
54. Powell, K.G., Roe, P.L., Linde, T.J., Gombosi, T.I., De Zeeuw, D.L.: A solution-adaptive upwind scheme for ideal magnetohydrodynamics. J. Comput. Phys. **154**(2), 284–309 (1999)
55. Re, B., Abgrall, R.: A pressure-based method for weakly compressible two-phase flows under a Baer-Nunziato type model with generic equations of state and pressure and velocity disequilibrium. Int. J. Numer. Methods Fluids **94**(8), 1183–1232 (2022)
56. Romenski, E.I.: Hyperbolic systems of thermodynamically compatible conservation laws in continuum mechanics. Math. Comput. Model. **28**(10), 115–130 (1998)
57. Romenski, E.I.: Thermodynamics and Hyperbolic Systems of Balance Laws in Continuum Mechanics, pp. 745–761. Springer US (2001)
58. Romenski, E.I., Belozerov, A.A., Peshkov, I.: Conservative formulation for compressible multiphase flows. Q. Appl. Math. **74**, 113–136 (2016)

59. Romenski, E.I., Drikakis, D., Toro, E.F.: Conservative models and numerical methods for compressible two-phase flow. J. Sci. Comput. **42**, 68–95 (2010)
60. Romenski, E.I., Reshetova, G., Peshkov, I.: Two-phase hyperbolic model for porous media saturated with a viscous fluid and its application to wavefields simulation. Appl. Math. Model. **106**, 567–600 (2022)
61. Romenski, E.I., Reshetova, G., Peshkov, I., Dumbser, M.: Modeling wavefields in saturated elastic porous media based on thermodynamically compatible system theory for two-phase solid-fluid mixtures. Comput. Fluids **206**, 104587 (2020)
62. Romenski, E.I., Resnyansky, A.D., Toro, E.F.: Conservative hyperbolic formulation for compressible two-phase flow with different phase pressures and temperatures. Q. Appl. Math. **65**(2), 259–279 (2007)
63. Romenski, E.I., Toro, E.F.: Compressible two-phase flows: two-pressure models and numerical methods. Comput. Fluid Dyn. J. **13**, 2 (2012)
64. Rusanov, V.: The calculation of the interaction of non-stationary shock waves and obstacles. USSR Comput. Math. Math. Phys. **1**(2), 304–320 (1962)
65. Saurel, R., Abgrall, R.: A multiphase Godunov method for compressible multifluid and multiphase flows. J. Comput. Phys. **150**(2), 425–467 (1999)
66. Scannapieco, A.J., Cheng, B.: A multifluid interpenetration mix model. Phys. Lett. A **299**(1), 49–64 (2002)
67. Schmidmayer, K., Petitpas, F., Daniel, E., Favrie, N., Gavrilyuk, S.: A model and numerical method for compressible flows with capillary effects. J. Comput. Phys. **334**, 468–496 (2017)
68. Tavelli, M., Dumbser, M.: Arbitrary high order accurate space-time discontinuous Galerkin finite element schemes on staggered unstructured meshes for linear elasticity. J. Comput. Phys. **366**, 386–414 (2018)
69. Thein, F., Romenski, E.I., Dumbser, M.: Exact and numerical solutions of the Riemann problem for a conservative model of compressible two-phase flows. J. Sci. Comput. **93**, 83 (2022)
70. Titarev, V.A., Toro, E.F.: ADER schemes for three-dimensional nonlinear hyperbolic systems. J. Comput. Phys. **204**(2), 715–736 (2005)
71. Toro, E.F.: Riemann Solvers and Numerical Methods for Fluid Dynamics. Springer, Berlin (2009)
72. Toro, E.F., Millington, R., Nejad, L.: Towards very high order Godunov schemes. In: Godunov Methods, Theory and Applications. Springer (2001)
73. Toro, E.F., Titarev, V.A.: Solution of the generalized Riemann problem for advection-reaction equations. Proc. R. Soc. Lond. A Math. Phys. Eng. Sci. **458**(2018), 271–281 (2002)
74. Toro, E.F., Titarev, V.A.: Derivative Riemann solvers for systems of conservation laws and ADER methods. J. Comput. Phys. **212**(1), 150–165 (2006)
75. Van der Waals, J.D.: The thermodynamic theory of capillarity under the hypothesis of a continuous variation of density. J. Stat. Phys. **20**(2), 200–244 (1979)
76. Zanotti, O., Fambri, F., Dumbser, M., Hidalgo, A.: Space-time adaptive ADER discontinuous Galerkin finite element schemes with a posteriori sub-cell finite volume limiting. Comput. Fluids **118**, 204–224 (2015)


## Authors and Affiliations


**Laura Río-Martín[1,2] · Michael Dumbser[1]**

✉ Michael Dumbser
michael.dumbser@unitn.it

Laura Río-Martín
laura.delrio@unitn.it

[1] Department of Civil, Environmental and Mechanical Engineering, University of Trento, Via Mesiano 77, Trento 38123, Italy

[2] Department of Information Engineering and Computer Science, University of Trento, via Sommarive 9, Povo, Trento 38123, Italy